Ecological Modelling 481 (2023) 110358

Contents lists available at ScienceDirect

Ecological Modelling

journal homepage: www.elsevier.com/locate/ecolmodel

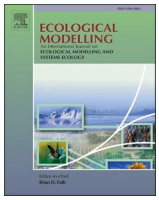

Modelling the spatial shifts of functional groups in the Barents Sea using a climate-driven spatial food web model

Marcela C. Nascimento [a,*], Berengere Husson [b], Lilia Guillet [b], Torstein Pedersen [a]

[a] Department of Arctic and Marine Biology, UiT The Arctic University of Norway, Hansine Hansens veg 18, Tromsø 9019, Norway
[b] Department of Ecosystem Processes, Institute of Marine Research, Bergen, Norway

ARTICLE INFO

Keywords:
Ecological modelling
Ecospace
Model validation
Spatial distribution shift

ABSTRACT

We built a dynamic, spatial food web model for the Barents Sea, developed with Ecospace by including species' habitat requirements and ecological interactions. The model was used to test the spatial shifts of different functional groups due to warming. We compared model-predicted and field-surveyed biomass of functional groups (FGs) spatial distributions in relatively cold and warm years. The Ecospace model included habitat foraging capacities for environmental parameters such as water temperature and bottom depth for 74 FGs out of a total of 108 FGs. We created two plausible scenarios, one representing a relatively cold year (2004) and another representing a warm year (2013) with differences of ca. 0.3 °C in bottom temperature, 0.6 °C in surface temperature, and 7% less ice coverage between them. Comparison of centre of gravity, inertia, and spatial overlap of the modelled and surveyed spatial distributions in warm and cold years showed that the model represented the past distributions of the functional groups satisfactorily. We observed poleward shifts of 41 and 68 km for the modelled and observed distributions, respectively, in the average centre of gravity position for the 35 FGs with lowest sampling uncertainty. The model predicted that the whole community had shifted distribution towards the northeast at an average rate of 4.4 km year^{-1} and 67 km °C^{-1} between 2004 and 2013. We conclude that our Ecospace model represents past observed species distributions in the Barents Sea satisfactorily, and may predict the direction and magnitude of temperature-driven changes in spatial distributions. This ability may be useful for predicting the impact of climate changes on species and FG distributions in future scenarios.

1. Introduction

Many marine species have changed their spatial distributions over the past few decades due to global climate change (Poloczanska et al., 2016). At high latitudes in the Barents Sea, poleward shifts of marine fish spatial distributions due to warming have been documented based on survey observations (Fossheim et al., 2015; Frainer et al., 2017). There is, however, less documentation of spatial shifts for other group of organisms that are less surveyed than fishes. In high latitude areas, changes in air and water temperature often co-occur with changes in ice coverage, light availability, open-water area, and primary production (Dalpadado et al., 2020; Pedersen et al., 2021; Reigstad et al., 2011). In the Barents Sea, pelagic primary production increased markedly with decreasing ice coverage (Dalpadado et al. 2020), and the associated changes in several environmental factors may complicate the evaluation of warming effects. Although a species' distribution is highly connected to environmental aspects, it also depends on the responses of its predators and prey to changes in environmental conditions and the availability of suitable habitats.

Marine species differ significantly in their thermal responses, with arctic species preferring low temperature and boreal species preferring higher temperature, as well as in the range of thermal tolerance, i.e., narrow (stenothermal) vs wide (eurythermal) responses (Pörtner and Gutt, 2016). Thus, spatial distribution responses to temperature changes are expected to depend on the thermal response of the species. Spatial models for components in marine ecosystems span in complexity from conceptual models (Nordøy et al., 2008) to statistical (Fall et al., 2018; Husson et al., 2020), species-distribution, individual-based models (Gonzalez-Mirelis et al., 2021; Huse et al., 2004), dynamic mass-balance (Slagstad and McClimans, 2005), and spatially resolved end-to-end models (Audzijonyte et al., 2019). Spatial modelling involving functional groups (FGs) at all trophic levels has been less common, though modelling approaches such as Atlantis and Ecopath with Ecosim and Ecospace (EwE) have such capacities (Audzijonyte et al., 2019; Fulton

* Corresponding author.
E-mail address: marcela.c.nascimento@uit.no (M.C. Nascimento).

https://doi.org/10.1016/j.ecolmodel.2023.110358
Received 31 August 2022; Received in revised form 7 February 2023; Accepted 10 March 2023

et al., 2018; Walters et al., 1999). Dynamic spatial models can represent the biological community and include species' habitat requirements (e.g., thermal responses) and ecological interactions. The dynamic spatial model Ecospace can incorporate environmental aspects of species' habitat foraging capacity and predator-prey relationships to drive changes in functional groups. This enables the model to reproduce the impact on abiotic conditions, spatially, according to the strong environmental gradient in the region and, temporally, on distribution of boreal and arctic species with different habitat preferences.

The EwE approaches model mass-balanced food webs based on the energy flows between FGs (Christensen et al., 2008). In this context, an FG may represent species, a sub-group of species, or a group of species that are functionally and ecologically similar. Based on this principle, Ecopath provides a static, mass-balanced snapshot of the system and is the base for the Ecosim and Ecospace approach (Christensen and Pauly, 1992; Polovina, 1984; Walters et al., 1997). Ecospace is the spatio-temporal framework that allows one, based on the trophic relationships, to answer temporally- and spatially-explicit ecological questions (Christensen et al., 2014, 2008; Walters et al., 1997).

In the Barents Sea, statistical and process-based models have been used in studies of how the modelled warming effects change the spatial distributions of some fish and zooplankton species (Huse and Ellingsen, 2008; Skaret et al., 2014). Spatial shifts due to warming are also expected in other areas. In an IPCC-based projection of a 3.7 °C increase in surface temperature and a 3.9 °C increase in bottom temperature off the North Atlantic coast of the USA, in the next 60–80 years, it is expected that target fishes will shift their distribution northward by about 100 to 200 km (Kleisner et al., 2017). Considering the average predicted increase in surface water temperature in the North Sea, Perry et al. (2005) estimated that two commercial fishes may retract entirely from the north of the North Sea by 2050, and other species may extend their range northward to encompass the entire region.

The Barents Sea is strongly influenced by the inflow of warm Atlantic water with temperature and flux that vary over time, with alternating warm and cold periods (González-Pola et al., 2020; Schlichtholz, 2019; Trofimov et al., 2019). However, over the past two decades, the water temperature has increased, and ice coverage has decreased more intensely (Ingvaldsen et al., 2021; Trofimov et al., 2019). In the Barents Sea, much information on the responses of FGs to environmental factors such as depth, temperature, bottom substrate, and ice-affinity is available from monitoring surveys, e.g., the integrated ecosystem surveys initiated in 2004 (Dolgov, 2016; Eriksen et al., 2018; Husson et al., 2020; Wienerroither et al., 2011). Information on responses of FGs to environmental factors can potentially be integrated into Ecospace habitat foraging functions, while comparing species using survey-based observation and modelled distributions could be helpful to evaluate the model results. It is expected that by including information on the responses of FGs to environmental factors, such as habitat capacity, the model will represent the FGs' distributions well. Due to the particular oceanic dynamics in the Barents Sea, with the influence of the warm Atlantic water from the southwest and the Arctic's influence from the north and northwest, it is expected that all FGs in the Barents Sea ecosystem will move poleward with an increasing temperature and a reduction in ice coverage.

Testing model predictions by confrontation with field-observed data early in the modelling process is essential to enhance model quality and avoid model misspecification (Jørgensen and Fath, 2011). However, few studies have evaluated marine spatial models' output by comparing model-predicted to field-observed spatial distributions; see attempts by Huse et al. (2004). Ecospace uses a spatial grid which may be adapted to the spatial resolution of field sampling to ease comparison of modelled and observed data. There are few studies in which Ecospace-modelled distributions are compared directly to field-observed distributions, though see Coll et al. (2019) and Romagnoni et al. (2015).

This work aimed to understand the effect of climate change on the spatial distributions of high-latitude marine biota. To do so, we developed an Ecospace model for the Barents Sea ecosystem from an already-published EwE model (Pedersen et al., 2021). Its performances were assessed based on the evaluation of its capacity to reproduce field-observed spatial distributions of the different FGs under two different climatic scenarios corresponding to a warm year (2013) and a relatively colder one (2004). Then the impact of warming was assessed through the measure of the shift in FGs distributions between the two years

2. Material and methods

2.1. Study area and Ecospace input data

The model represents the Barents Sea Large Marine Ecosystem (LME), latitude minimum 63° 48′ 13″ N and maximum 82° 57′ 57.7″ N, longitude minimum 0° 51′ 48.3″ W and maximum 68° 8′ 12″ E (Marine regions, 2022), extending from the Norwegian Sea and eastwards to Novaya Zemlja and northwards from the coast of Norway and Russia (Drinkwater, 2011), covering an area of 2.01 million km^2 (Skjoldal and Mundy, 2013) (Fig. 1).

The Barents Sea is a relatively shallow shelf sea (Ozhigin et al., 2011) with an average depth of about 230 m. The most profound areas deeper than 400 m are in the western part (Loeng and Drinkwater, 2007). The Barents Sea receives warm Atlantic water (above 2 °C) and coastal waters (above 3 °C) from the southwest (Loeng and Drinkwater, 2007) as well as some cold Arctic water with temperatures below 0 °C from the north and east (Hunt et al., 2013). The polar front is the transition zone between the warmer boreal southern part and the colder Arctic northern area (Loeng, 1991) (Fig. 1). The Barents Sea is seasonally ice-covered; the maximum ice coverage occurs in March–April, and the minimum in August–September (Drinkwater, 2011).

The spatial distribution of organisms in the studied area reflects the climatic gradient within the Barents Sea (Andriyashev and Chernova, 1995; Jørgensen et al., 2015; Renaud et al., 2018) and, during the recent warm period boreal fish species have generally expanded northwards at the expense of arctic species (Fossheim et al., 2015). The modelling design uses Ecopath-included data input from field surveys and literature and is summarised in Fig. 2.

2.2. Ecosystem survey

The joint Ecosystem Survey run by the Institute of Marine Research (IMR) and Polar Research Institute of Marine Fisheries and Oceanography (PINRO) (Eriksen et al., 2018; Prozorkevich et al., 2020) aims to monitor the status of abiotic and biotic factors and changes in these in the Barents Sea ecosystem. It was initiated in 2004 and conducted annually in the autumn until the present day, gathering a considerable amount of data about the Barents Sea ecosystem.

Data for species distribution used in this study came from the Campelen 1800 bottom trawl (22 mm mesh size at cod end), which captures demersal and bathypelagic species, as well as epibenthic megafauna as bycatch at a towing speed of approximately 3 knots. Only stations from 50 to 500 m depth towed between 15 and 60 min were kept, so as to ensure a homogeneous sampling of the offshore Barents Sea ecosystem. An average of 278 stations are sampled yearly in a grid design of 64.8 km mesh size, covering south and west of Svalbard to Franz Joseph Land and Novaya Zemlya. During the surveys, the catch per unit effort (CPUE) is calculated for each taxon and station by standardising species' biomass by unit sampling area.

2.3. Ecospace and Ecopath with Ecosim base model

The model is based on an Ecopath with Ecosim calibrated model (Pedersen et al., 2021), representing the ecosystem of the Barents Sea LME in the year 2000. The model comprises 108 FGs representing mainly boreal and arctic species (for more details see Pedersen et al.,

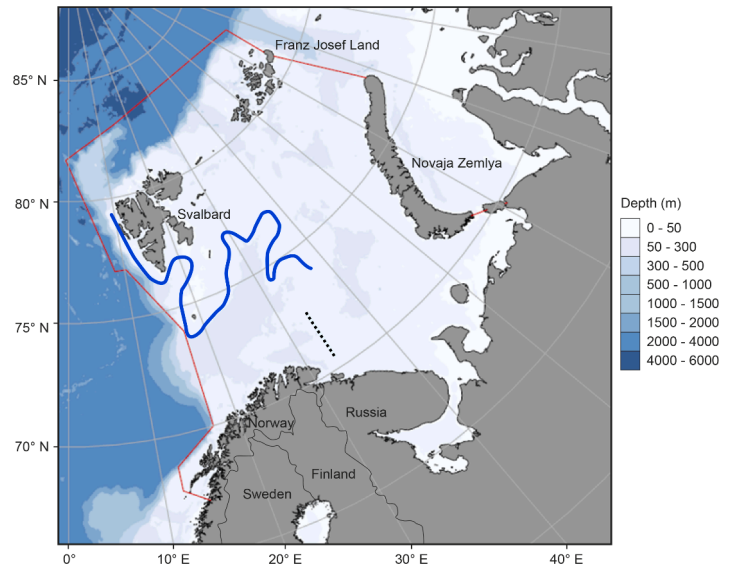

Fig. 1. Map of Barents Sea Large Marine Ecosystem. Borders of the ecosystem are shown in red lines (based on https://www.pame.is/projects/ecosystem-approach/arctic-large-marine-ecosystems-lme-s). The Kola transect for hydrographic monitoring is shown as a black dotted line, and the polar front position based on Loeng (1989a) is shown as a blue line.

2021). The Ecosim model has been fitted (calibrated) to a time-series for the period 1950–1996 to estimate predator-prey vulnerabilities (Pedersen et al., 2021), and these vulnerabilities have been carried over to the Ecospace model. The Ecopath and Ecosim model described in Pedersen et al. (2021) showed that the basic ecosystem structure was preserved during the periods of overexploitation between 1970 and 1990 and during the recovery after 1990. This resilience is expected to be reflected in the stability of FGs' spatial distributions modelled by Ecospace. Another important aspect highlighted by Pedersen et al.'s (2021) model is the increase in productivity at lower trophic levels during warm years, leading to higher productivity for most high trophic level FGs, which is likely to impact the FGs spatial distributions.

The Ecospace model applies a two-dimensional grid (basemap). The basemap identifies the spatial bounds and grid dimensions, and includes the modelled area's environmental characteristics, defined habitats, and FG environmental limits (Christensen et al., 2014, 2008). Based on the temporal equations, Ecospace models the biomass of each FG within each cell in the grid over time by considering trophic interactions, fishing, and species' movement (Christensen et al., 2008; Walters et al., 1999). The habitat foraging capacity concept included in Ecospace aims to increase the model's realism, making the food web interact effectively and spatiotemporally with the environmental variability (Christensen et al., 2014).

The model ran with monthly time steps and the simulation time was set to 20 years. To define the Ecospace maps, we used the same projection as the joint Ecosystem Survey, with a cell grid of square cells of 64.8 km in length and width. The spatial environmental drivers (i.e., a value of the driver for each grid cell) included depth, bottom and surface temperature, days of ice coverage, the distance off the coast (Buhl-Mortensen et al., 2015; Lien et al., 2013), and primary production (Reigstad et al., 2011).

We constructed this model using the Ecopath with Ecosim and Ecospace software version 6.6.6 (Christensen et al., 2008). The model allocated the biomasses of the FGs dynamically across a two-dimensional grid map with 32 cells in the longitudinal direction and 28 cells in the latitudinal direction, giving a total of 486 active cells (Fig. 3). The model calculated the FGs biomass spatial distributions based on FGs' habitat foraging capacities, predation regimes, dispersal rates, and the spatially-resolved environmental input (Christensen et al., 2014; Walters et al., 1999).

The dispersal rate parameters needed in Ecospace are the average annual movement distances (of random movement) of the FGs across the ecosystem (Christensen et al., 2008). For this model, we specified seven different dispersal rate values, representing the mobility of various FGs based on their movement patterns. The choices of values for each dispersal rate were based on previous studies (Mackinson and Daskalov, 2007; Püts et al., 2020; Romagnoni et al., 2015), as were the characteristics of all organisms in each FG and the environmental condition of the Barents Sea LME. We set 1000 km year^{-1} for fast top predators and highly migratory mammals and birds; 600 km year^{-1} for pelagic and migratory demersal FGs; 300 km year^{-1} for faster moving demersal fishes FGs and pelagic advected FGs; 200 km year^{-1} for snow crabs and coastal cod; 100 km year^{-1} for red king crab, which is a mobile crab; 30 km year^{-1} for benthic invertebrates and detritus FGs; and 10 km year^{-1} for offal (**Appendix A**).

2.4. Derivation of habitat capacity functions

The Ecopath model is run based on a system of linear equations describing the average mass and energy flows between all FGs during a period of time (Christensen and Pauly, 1992). In the temporal dynamic framework of Ecopath, Ecosim simulates the ecosystem effects of changes in mortality and environmental forces (Christensen and Walters, 2004). The consumption rates are calculated based on the foraging arena concept, where biomasses are divided into vulnerable and invulnerable components (Ahrens et al., 2012).

The Ecospace time-spatial model works based on the Ecosim set of equations, predicting the biomass dynamics in the two-dimensional grid map (Walters et al., 1999). Each active cell can contain one or more habitat type and environmental driver, such as water temperature and bottom depth. These habitat types can affect the computed foraging capacity of the FGs, implemented via separate environmental preference functions for each environmental parameter calculated for each cell. This procedure allows more variation amongst the cells to distribute the FGs over the map where they are most likely to occur (Christensen et al., 2014).

The habitat foraging capacity is based on the foraging arena theory (Ahrens et al., 2012). The computed habitat foraging capacity is calculated from FGs affinity for given habitats and functional responses to environmental conditions based on the habitat layers in the basemap. Each habitat type gets a proportion assigned according to how suitable it is for a certain FG (Christensen et al., 2014). Environmental capacity is

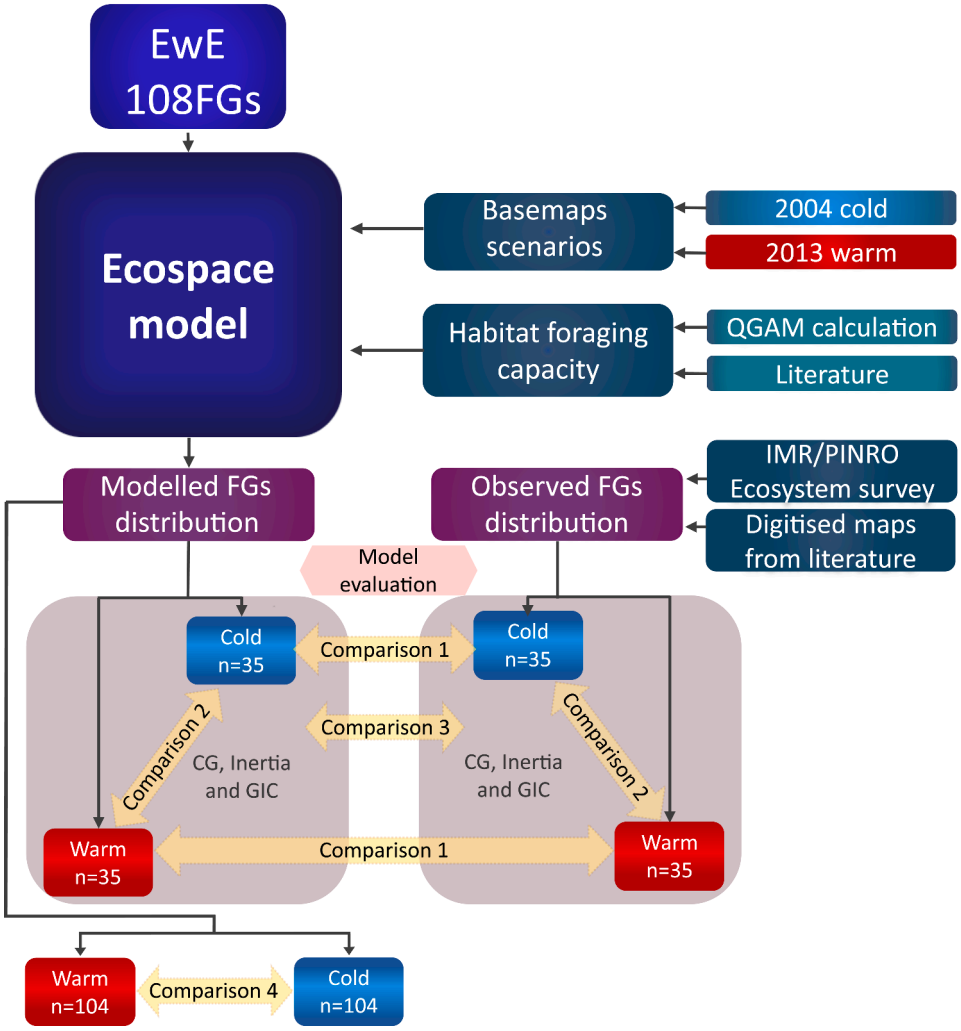

Fig. 2. Diagram of the workflow and results of the main analysis. Comparison 1 is between the modelled vs observed distributions in the cold and warm scenario. Comparison 2 is between cold and warm scenarios for modelled and observed distributions. Comparison 3 is shifts in distributions from cold to warm scenarios between modelled and observed. Comparison 4 is between modelled cold and warm scenarios for the whole community.

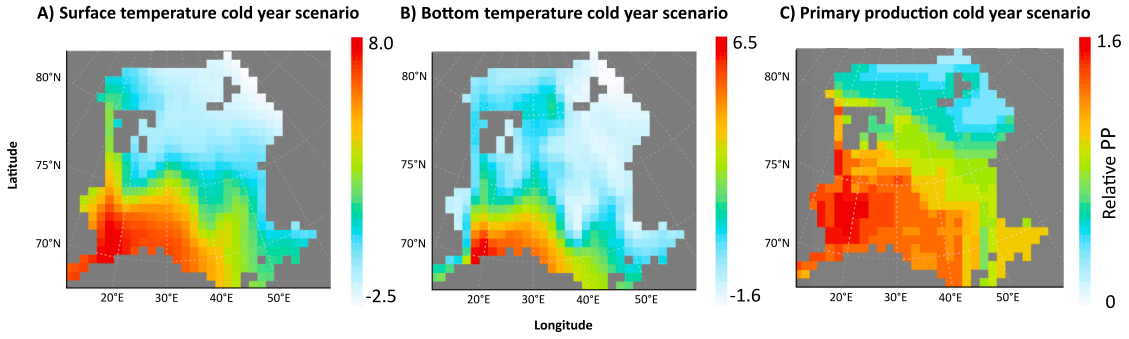

Fig. 3. Overview of basemaps of the 2004 scenario (cold year) showing A: the surface temperature (Nordic Seas 4 km numerical ocean model hindcast archive - SVIM); B: the bottom temperature (SVIM); and C: the primary production based on Reigstad et al. (2011), representing the primary production (PP) relative to the Ecopath PP baseline of the Barents Sea LME.

based on environmental driver maps. It enables the model to drive the FGs' foraging capacity from the cumulative effects of multiple physical, oceanographic, environmental, and topographic conditions spatially and runs in conjunction with the food web and fisheries dynamics (Coll et al., 2019).

We used two approaches to derive habitat capacity functions: i) the quantile generalised additive model (QGAM) approach for FGs with sufficient survey data from the Ecosystem Survey with data from 2004 to 2019; and ii) literature information on environmental preferences. For the habitat capacity based on data from the Ecosystem survey, we calculated one QGAM (Husson et al., 2020) per species-habitat variable couple using the QGAM package in R (Fasiolo et al., 2017).

The QGAM is a generalised additive model (GAM) for which the fitted target is a chosen quantile rather than the mean. When fitting the

99th quantile, we thus estimated the maximum possible biomass for each FG in response to each environmental variable. This amounted to calculating a potential niche for each FG (Cade et al., 2005). We used the same methodology as Husson et al. (2020). The number of degrees of freedom in the QGAMs was limited to three in order to avoid complex regressions without ecological rationality. To evaluate the predictive power of each QGAM model, all results were fitted using a training dataset consisting of observations for the years 2004 to 2013. They were then evaluated on the testing dataset, which included observations for the years 2014–2019.

To extract distribution parameters to be used as habitat foraging capacities for each FG in Ecospace, we fitted alternative classical continuous distribution curves: logistic, beta, log normal, exponential, and normal using the fitdistrplus (Delignette-Muller and Dutang, 2015), logspline (Charles et al., 2002), betareg (Cribari-Neto and Zeileis, 2010), and extraDistr (Wolodzko, 2019) packages in R on each QGAM species-environment model. In addition, we estimated binormal distributions, which is one of the possible shapes of habitat capacity function in Ecospace. It comprises two half-normal distribution functions specified by three parameters: the mean, the left, and the right standard deviation halves of normal distributions. The left half distribution fits the data below the mean and the right half distribution fits the distribution above the mean. The binormal distribution can approximate various function shapes ranging from ordinary normal distribution to sigmoid-shaped relationships. We adjusted functional relationships between habitat capacity, and temperature and depth for some groups based on QGAM results to follow the observed distribution (Fig. 4, **Appendix B**). Habitat capacity functions varied widely between FGs depending on the relationship between the FGs and the environmental drivers (Fig. 4).

Most habitat capacity functions were entered as binormal distributions (for more details, see **Appendices B and C**). However, the 'ice coverage' functions were entered as right shoulder function when the FG was more dependant on the ice, and left shoulder when the FG was assumed to avoid the ice. A beta function was used for ice coverage for crangonid shrimp. The distance off the coast was entered as an exponential function with decreasing habitat capacity with increased distance from the coast.

To derive literature-based habitat capacity relationships for the FGs that were not well represented in the Ecosystem survey results, we also included habitat capacities derived from published studies on spatial distributions as well as environmental preferences and tolerances. The Ecosystem Survey is conducted in autumn, the warmest months of the year, and therefore the survey does not cover the entire niche of the species. We included habitat capacity for 74 FGs, with 29 FGs using habitat capacities based on QGAM estimations and 45 FGs using habitat capacities based on literature and personal observations (for more details, see **Appendix C)**.

The foraging capacity of FGs that were dominant in terms of biomass at its trophic levels were included sequentially one by one, followed by a comparison of the observed and modelled distributions of all FGs. This process was repeated until all FGs, including those with no habitat capacity, had a modelled distribution similar to the observed, by including as few as possible habitat capacities so as to avoid overfitting the model. The QGAM calculations for 28 FGs, mainly commercial fishes caught by bottom trawl, indicate that depth, bottom, and surface temperature, and ice coverage can be good predictors for the distribution of most evaluated FGs. Fig. 4 shows an example of habitat capacities included in Ecospace as foraging capacity. Fig. 4**A** shows the temperature capacity for arctic (polar cod), arctic boreal (Northeast Arctic cod), and boreal (blue whiting) FGs. Fig. 4**B** shows the depth capacity for shallow (large bivalves), intermediate (pelagic amphipods), and deep (sperm whale) FGs.

2.5. Scenario set-ups for cold and warm years

The year 1990 marked the beginning of the most recent warm period in the Barents Sea region (Trofimov et al., 2019). In the mid-2000s the warming condition amplified (Schlichtholz, 2019). The species and FGs are expected to be affected by these environmental changes, and we expected that this model would be able to perform the calculations. However, to evaluate whether our model could represent the natural variability of the environmental conditions in the Barents Sea and FGs during the warming conditions of the past two decades, we specified two scenarios in Ecospace. One represented a warm and another a less-warm or cold year within the warm period, with differences in water temperature and ice coverage between the scenarios described below.

Within the warm period from the beginning of the Ecosystem Survey onwards, the coldest year in the Kola section (Fig. 5) water column temperature time-series was 2011, and the warmest was 2012 (Fig. 5) (González-Pola et al., 2020). However, in order to validate the model, data from field observations were necessary, and the years that combined the best-observed data, the most extensive geographic coverage, and adequate environmental conditions were the cold 2004 and warm 2013.

Spatial environmental information for this model was taken from the

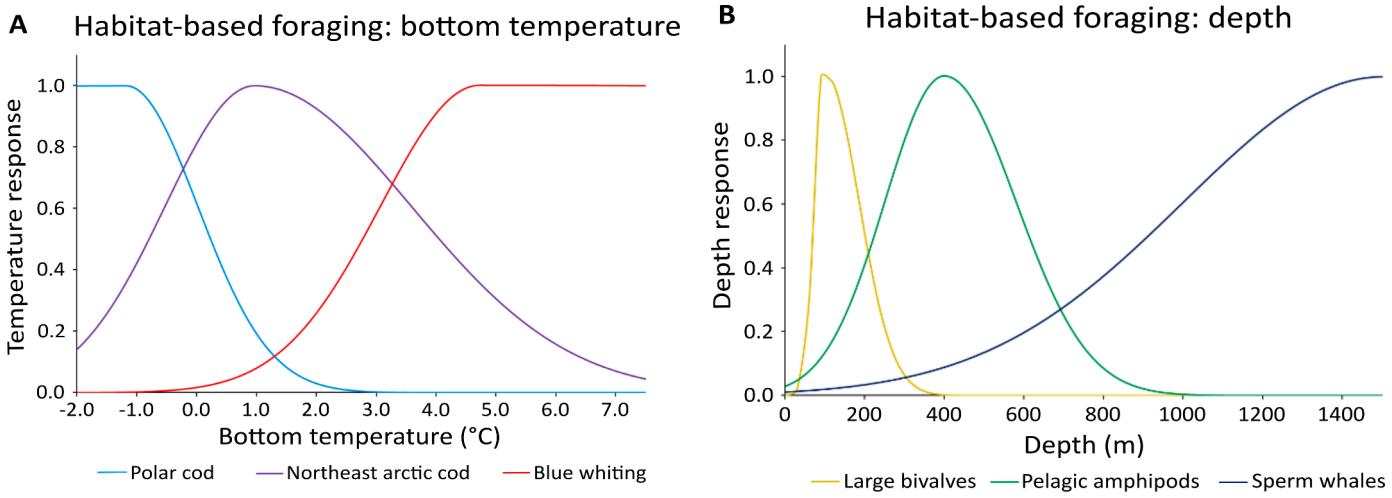

Fig. 4. Examples of habitat capacity functions for bottom temperature (A) and bottom depth (B) for functional groups with different responses in the Barents Sea Ecospace model. Temperature response is shown for arctic (polar cod), arctic-boreal (Northeast Arctic cod), and boreal (blue whiting) FGs, and depth response for FGs preferring shallow (large bivalves), intermediate (pelagic amphipods) and deep (sperm whale) waters. See Appendix C for background data.

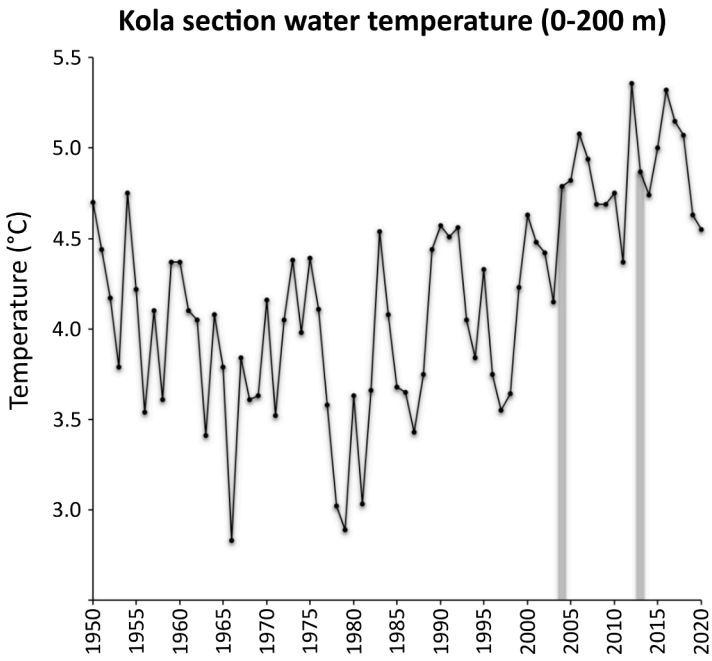

Fig. 5. Average water column temperature in the Kola section (0–200 m depth). The line with the dots represents the historical data, and the grey bars show the years with spatial environmental data from the SVIM archive used in Ecospace for a relatively cold (2004) and warm (2013) year (values in Appendix D Table D1).

Nordic Seas 4 km numerical ocean model hindcast (SVIM) archive, a numerical ocean model hindcast that simulates the Nordic and Barents seas at a spatial resolution of 4 km (Lien et al., 2013). This model was developed from 1960 to 2011 and represents the Barents Sea's physical environment well (Lien et al., 2013). However, it is annually updated and validated by observed data and provides continuous information about these areas' environmental conditions. According to the SVIM -archive, the average annual surface temperature for the Barents Sea in 2013 was 0.57 °C warmer than in 2004, and the average bottom temperature in 2013 was 0.27 °C higher than in 2004 (**Appendix D,** Table D1). We constructed two temperature scenarios, one for the relatively cold (2004) (Fig. 3) and another for the warm (2013) year based on SVIM archive.

In Ecospace, functional groups can move to the four adjacent cells through random-directional movements mediated by habitat preferences and responses of organisms to depredation risk and feeding conditions (Christensen et al., 2014). In order to define the FG habitat preferences, it is necessary to include basemaps that can embrace many environmental aspects. The present study included depth, bottom temperature, surface temperature, ice coverage, the distance off the coast, and sediment type (gravel, sand and mud, pebbles, and rocky bottom) (**Appendix E**).

The scenarios were constructed based on the annual average values of each cell in the maps for the bottom and surface water temperature and ice coverage. The average, minimum, and maximum values of the scenario basemaps can be seen in **Appendix D**, Table D1. For phytoplankton primary production, we digitised maps based on Reigstad et al. (2011) for the relatively cold (1998) and warm (2006) years. For the distance off the coast basemap, we built a map defining the ranges of distances 64.8 km, 129.6 km, 194.4 km, 259.2 km, 324 km, and 388.8 km from the coast, which are the distances of the cells in the grid from the closest to the coast to the more distant.

In addition to the environmental drivers, habitats may be specified in Ecospace assets of (water) cells sharing certain features affecting the movements, feeding rate, and survival of the Ecopath model components occurring therein (Christensen et al., 2008). All habitat maps for the substrate category were derived from MAREANO – The Sea in Maps and Pictures (Buhl-Mortensen et al., 2015). The MAREANO seabed map for substrate (grain size) has a higher resolution than our model grid, and we classified it into four discrete categories: gravel, sand and mud, pebbles, and rocky bottom (**Appendix E).**

2.6. *Comparison of modelled and survey-based spatial distributions*

To evaluate the performance of the Ecospace model for the Barents Sea, we compared the modelled and survey-observed distributions for a total of 35 FGs with good spatial distribution data available for warm and cold years encompassing the whole LME Barents Sea (**Appendix F**).

Two major sources for spatial distributions were used. For 28 FGs, we obtained observed spatial distributions of biomass from the Ecosystem Survey for 2004 (cold) and 2013 (warm). For FGs ($n = 7$) with spatial data from the Ecosystem Survey in 2013 but with no information for 2004, we used information from 2010 to represent a colder year than 2013. We also digitised distributions for 20 FGs from published papers (**Appendix D** Table D2) to the same projection we used for the Ecospace basemap (projection = aea, datum based on Hayford (1909), and unit = m*)*.

To convert the published distributions of original maps to raster maps at the same projection and scale as the Ecospace basemap, we used an image of the original map in GIF format. Using the open-source Quantum Geographic Information System (QGIS) and its raster tool georeferencer, we adjusted the figure with the projection used in the Ecospace basemap. We transferred the values from the TIFF image with a grid generated by the QGIS to a raster file with basemap dimensions and then plotted it using R (RStudio, 2021). See the digitalised maps in **Appendix E.**

To evaluate the uncertainty in the resulting spatial grid matrices, we allocated the spatial distributions into uncertainty categories according to the origin and quality of the spatial distribution data using a score ranging from 1 (lowest uncertainty) to 5 (highest uncertainty) (Table 1 and **Appendix F**).

To compare the observed distributions from warm and cold years with the modelled distributions for 2004 and 2013 produced by the Ecospace model, we calculated the centre of gravity and inertia for each FG. Centre of gravity (CG) is the mean geographical location of the biomass distribution of the FG, and inertia is the spread (variance) of the

Table 1
Categories of the uncertainty score of the data collection of the observed distribution of the FG.

Uncertainty score	Assumed uncertainty	Description	FGs
1	Lowest	FGs composed mainly of one species with sampling designed for that species and collected with appropriate gear.	Northeast Arctic cod (+3), saithe (3+), haddock (3+), capelin age 3+, Polar cod age 2+, blue whiting, large redfish
2		FGs composed of species with the appropriated collection and gear, but the collection was not designed for that species, or mixed FGs comprised of few species with good data collection and the species with good data sampling converted from literature.	Wolffishes, thorny skate, long rough dab, lumpfish, cephalopods, scyphomedusae, chaetognaths, *Thysanoessa*, large krill, medium-sized copepods, northern shrimp
3		Represented mainly by mixed FGs (comprised of many species), with few representatives with excellent or good sampled data, or well-sampled groups with mixed ages, e.g., cod 0–2 (average of 0–group data and adult data).	Northeast Arctic cod (0–2), saithe (0–2), haddock (1–2), other small gadoids (Norway pout), Stichaeidae (daubed and snake blenny), other large benthic invertebrate feeding fishes (Arctic skate), Small herring, capelin age 0–2, small redfish, snow crab
4		Mainly mixed FGs, with few representatives with excellent or good sampled data, and well-sampled groups with mixed ages, e.g., cod age 0–2 (average of 0–group data and adult data).	Large Greenland halibut, small Greenland halibut, other benthivore flatfish (lemon sole and plaice), crangonid and other shrimps, other large crustaceans, predatory asteroids, detrivorous polychaetes
5	Highest	Possible to compare in general, but showing gaps that made the comparison less reliable, e.g., without separation between cold and warm year distribution or not covering the same area.	All other FGs

distribution of the observed and modelled distributions (Woillez et al., 2007, 2009). To evaluate how the FGs spatial distribution overlapped, we calculated the global index of collocation (GIC). The GIC was calculated by comparing the distance between the CGs of a pair of FGs and their respective inertias (Woillez et al., 2007, 2009). The GIC ranges from 0, when each distribution is concentrated in a single and different location, to 1, when the CGs of the two distributions coincide.

To evaluate how distant the observed spatial distributions are from the modelled distributions, we calculated the distance in km between the observed and the modelled centre of gravities for FGs based on the Pythagorean theorem. The angular deviation between observed and modelled distributions' CGs was calculated using the arctangent of the observed and modelled CG difference. It was then converted to degrees on a 360° scale (azimuth). The same procedure was repeated to analyse the differences in FGs' distribution between cold and warm years.

To assess the main direction of spatial shifts, a clockwise circle centred on the modelled CGs was split into four equal quadrants: northeastern between 0° and 90°; southeastern between 90° and 180°; southwestern between 180° and 270°; and northwestern between 270° and 360°. Frequencies of FGs within each quadrant were compared, and this compartmentation allowed us to define the main direction of dislocation between modelled and the observed survey-based distribution. Here, we set the results as the azimuth, an angle between 0° and 360° measured clockwise from the north, and bearing, that is, an angle lower than 90° within a quadrant defined by the cardinal directions. To evaluate the main shift of CGs from the cold year to the warm year, we calculated the average directional shift of all modelled and observed CGs.

Chi-square tests were applied on contingency table data to test if frequencies of directions of CG differed between north and south, east and west, or between quadrants, and a significance level of $\alpha = 0.05$ was applied (Zar, 1998). The Kruskal-Wallis (KW) test was used to test if distributions of a variable were equal in more than two groups.

To evaluate if the habitat overlap patterns of predators and prey in the modelled and observed distributions were similar, we calculated the GIC of all 35 predators' FGs and their primary prey FGs with available distributions for cold and warm years. The shift rate (km year^{-1}) between the CG position from cold to warm years was calculated by dividing the distance between the CG position from cold to warm year by the time interval in years.

2.7. Evaluation of changes in the Barents Sea community distribution in the past decade due to warming conditions

To evaluate changes in the modelled Barents Sea biological community due to the observed warming conditions over the past two decades, we calculated the average CG position of all modelled FGs in the cold (2004) and warm (2013) years and compared the distance and the bearing between them as described above. We then divided the distance from the 2004 to 2013 average CG position by the time interval and the difference in the water temperature (bottom and surface) from these two years to find the shift rate.

2.8. Thermal responses and distribution area

For each FG we applied Aquamaps' (Kaschner et al., 2019) parameter of surface temperature, and used the 10th quantile as the minimum and 90th quantile at maximum of the trapezoid function as a measure of width of the thermal response. This width is expected to be small for **stenothermal** species with narrow thermal tolerances, and large for **eurythermal** species that have broad thermal flexibility (Pörtner and Gutt, 2016). We allocated FGs to biogeographical categories with **arctic** species as those with a maximum limit (90th) of 8 °C and the lower limit below 0 °C; **arctic-boreal** were the species with the minimum (10th) around 0 °C, the maximum (90th) around 10 °C, and the absolute maximum up to 12 °C; **boreal** were species with the minimum (10th) higher than 4 °C and maximum (90th) lower than 14 °C; and **broad** were the species with the range between the minimum (10th) and maximum (90th) embracing the arctic and boreal limits and beyond.

To represent the area of the FGs distribution, we calculated the inertia area then divided the inertia of the modelled FGs' warm year by the cold year and observed if the area increased, decreased, or remained stable. Then we compared the inertia area of all modelled FGs using the paired Wilcoxon test comparing cold (2004) and warm (2013) year scenarios. To compare the variation of the modelled area amongst the four biogeographical groups and the three thermoplasticity groups from the cold (2004) and the warm (2013) year, we calculated the average difference of the inertia area by group and then compared them using the KW test.

3. Results

3.1. Comparison of modelled and observed distributions within cold and warm years

The FGs' distributions generated by the Ecospace model in cold and warm years were generally similar to the available observed distributions. Modelled and observed centres of gravity and inertia of FGs had similar values for most groups (Table 2 and **Appendix G**). Generally, the modelled distributions of FGs showed high spatial overlap with the observed distributions, with the average values for the global index of collocation (GIC) between modelled and observed distributions of 0.89 in cold and 0.88 in warm years (Table 2). An example of this is *Thysanoessa* (small krill), with a GIC of 0.87 for the cold and a GIC of 0.81 for the warm years (Fig. 6).

In the cold year scenario, the majority (57%) of CGs for observed distributions were located south of modelled distributions of CGs, and in the warm year scenario, most (60%) were located north of the modelled distributions of CGs (Table 2, Fig. 7, Fig. 8). However, the frequencies of northerly or southerly directions of differences between modelled and observed CGs in the cold or warm year scenario did not differ significantly ($\chi^2 = 2.06$, df = 1, $p = 0.15$). The frequencies of eastward or westward directions of differences between modelled and observed CGs in the cold or warm year scenario did not differ significantly ($\chi^2 = 0.23$, df = 1, $p = 0.63$). Neither were there significant higher frequencies of differences between modelled and observed CG in the northerly or southerly direction for the cold ($\chi^2 = 0.71$, df = 1, $p = 0.40$, Fig. 8) or the warm scenario ($\chi^2 = 1.40$, df = 1, $p = 0.24$, Fig. 8).

The frequencies of directions for the difference between modelled and observed CG in the various quadrants did not differ significantly between the cold and warm scenarios ($\chi^2 = 5.25$, df = 3, $p = 0.15$, Table 2, Fig. 7). In the cold year scenario, the frequencies in the quadrants did not differ significantly ($\chi^2 = 3.29$, df = 3, $p = 0.35$, Fig. 8). The distance between the modelled and observed CGs for each FG were less than 250 km for most FGs, except for six FGs which had distances up to 444 km (Table 2, Fig. 7). In the warm year scenario, 20% of the observed CGs were located northeast of the modelled CGs, 20% were southeast, 20% southwest, and 40% were northwest (Table 2, Fig. 8), though the frequencies in the quadrants did not differ significantly ($\chi^2 = 4.2$, df = 3, $p = 0.24$, Fig. 8). Most of the CGs in observed warm years were located less than 300 km from the modelled CGs (Fig. 7), except for seven FGs which had distances up to 429 km (Table 2).

The median distance between the CG for modelled and observed distributions was most prominent for the FG with the highest

Table 2
Functional groups (FGs) with good observed survey spatial distribution data for both warm and cold years for the Barents Sea as a whole, and compared with the modelled distribution in cold and warm years. GIC is the global index of collocation (overlap index between modelled and observed distribution). Distance is the distance between the modelled and observed centre of gravity, azimuth is the angle of the dislocation between the modelled (origo) and observed centres of gravity, and bearing is the angle of the dislocation between the modelled (origo) and observed centres of gravity divided by the direction into four quadrants of 90°

FG Number	FG Name	GIC		Distance (km)		Azimuth (degrees 360°)		Bearing (NE, SE, SW, NW)			
		Cold (2004)	Warm (2013)	Cold (2004)	Warm (2013)	Cold (2004)	Warm (2013)	Cold (2004)		Warm (2013)	
29	Northeast Arctic cod (3+)	0.91	1.00	217	47	175	338	5	SE	22	NW
30	Northeast Arctic cod (0–2)	0.91	0.94	209	170	206	271	26	SW	89	NW
33	Saithe (3+)	0.93	0.67	99	206	240	270	60	SW	90	SW
34	Saithe (0–2)	0.82	0.89	189	142	82	339	82	NE	21	NW
35	Haddock (3+)	0.86	0.85	225	256	102	54	78	SE	54	NE
36	Haddock (0–2)	0.97	0.84	89	251	21	4	21	NE	4	NE
37	Other small gadoids	0.66	0.72	248	210	256	253	85	SW	83	SW
38	Large Greenland halibut	0.74	1.00	387	28	341	300	19	NW	60	NW
39	Small Greenland halibut	0.65	0.74	411	358	302	296	58	NW	64	NW
41	Wolffishes	0.92	1.00	202	41	130	154	50	SE	26	SE
42	Stichaeidae	0.94	0.94	183	186	318	334	42	NW	26	NW
44	Other large bent invertebrate feeding fish	0.99	0.93	77	171	86	53	86	NE	53	NE
45	Thorny skate	1.00	0.99	28	63	204	134	24	SW	46	SE
46	Long rough dab	0.91	0.96	203	138	190	154	10	SW	26	SE
47	Other benthivore flatfish	0.67	0.68	444	407	170	209	10	SE	29	SW
49	Small herring	0.85	0.97	165	48	69	231	69	NE	51	SW
50	Capelin (3+)	0.85	0.81	241	324	291	314	69	NW	46	NW
51	Capelin (0–2)	0.97	0.77	110	273	255	237	75	SW	57	SW
52	Polar cod (2+)	0.96	0.80	115	254	313	326	47	NW	34	NW
54	Blue whiting	0.94	0.79	101	216	295	305	65	NW	55	NW
57	Lumpfish	0.93	0.93	174	179	249	282	69	SW	78	NW
59	Large redfish	0.92	0.97	139	96	253	302	76	SW	58	NW
60	Small redfish	0.94	0.96	121	107	268	318	88	SW	42	NW
62	Cephalopods	0.94	0.89	174	232	222	196	42	SW	16	SW
63	Scyphomedusae	0.94	1.00	175	37	262	285	82	SW	75	NW
64	Chaetognaths	0.96	0.88	155	296	223	150	43	SW	30	SE
65	*Thysanoessa*	0.87	0.81	238	304	223	195	43	SW	15	SW
66	Large krill	0.98	0.87	70	220	0	64	0	NE	67	NE
71	Medium sized copepods	1.00	0.97	42	165	90	286	90	NE	74	NW
79	Northern shrimp (*Pandalus borealis*)	0.98	0.99	104	67	77	133	77	NE	47	SE
80	Crangonid and other shrimps	0.86	0.81	302	359	99	86	81	SE	86	NE
81	Other large crustaceans	0.83	0.93	290	201	119	100	61	SE	80	SE
83	Predatory asteroids	0.76	0.68	367	429	82	81	82	NE	81	NE
87	Detrivorous polychaetes	0.97	0.97	103	111	33	4	33	NE	4	NE
101	Snow crab	0.87	0.76	217	309	101	97	79	SE	87	SE
	Average	0.89	0.88	189	197						
	SD	0.10	0.10	102	110						

The distances between centres of gravity for the modelled and observed FGs distributions were on average 189 km (SD = 102 km, $n = 35$) and 197 km (SD = 110 km) in the cold and warm scenario, respectively.

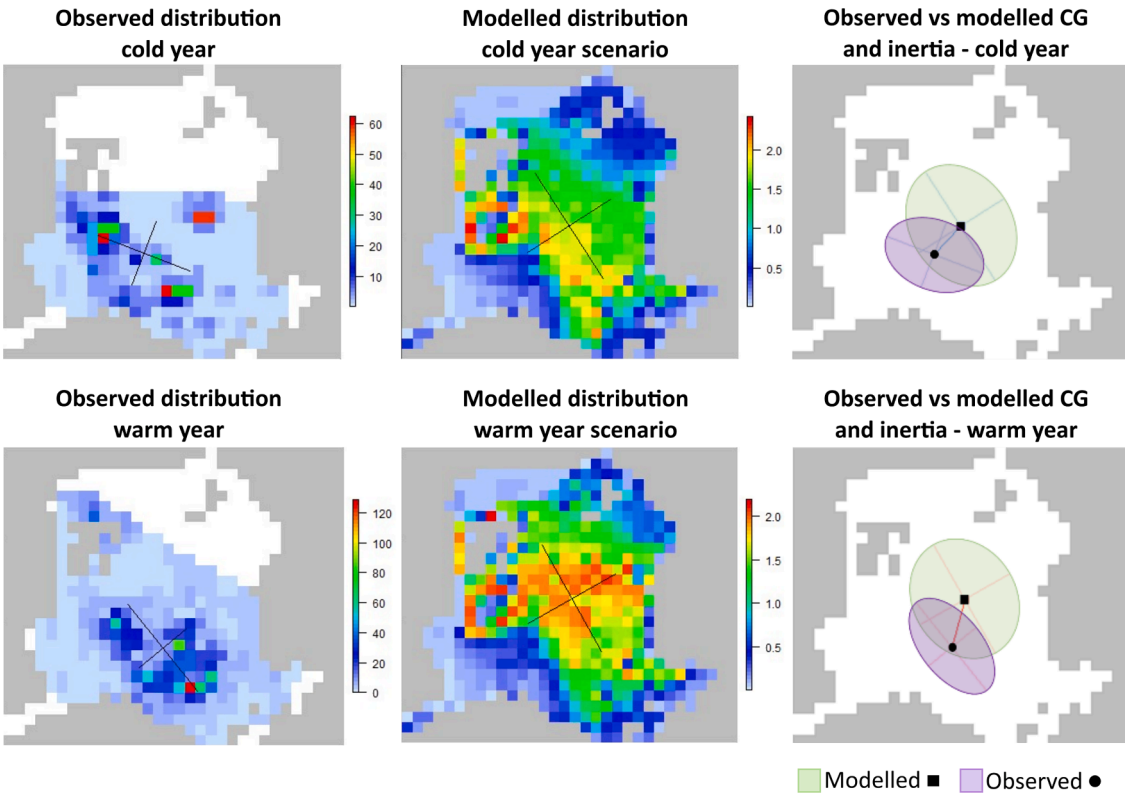

Fig. 6. Comparison of survey-observed and modelled spatial distributions of the krill Thysanoessa and its centre of gravity and inertia. Observed unit, based on Eriksen and Dalpadado (2011); Mikhina et al. (2019); Orlova et al. (2010), is wet weight in g m^{-2}. and Modelled by Ecospace (unit is carbon in g m^{-2}) the distribution of Thysanoessa (FG 65) shows a high overlap index (GIC) between cold (GIC is 0.87) and warm (GIC is 0.81). The squares and circles represent the centre of gravity of the modelled observed distributions, respectively. The green and purple ellipses represent the inertia of the modelled and observed distribution, respectively, and the crosses inside the ellipses represent the maximum inertia (long axis) and the minimum inertia (short axis). For the maps' georeference, see Fig. 3.

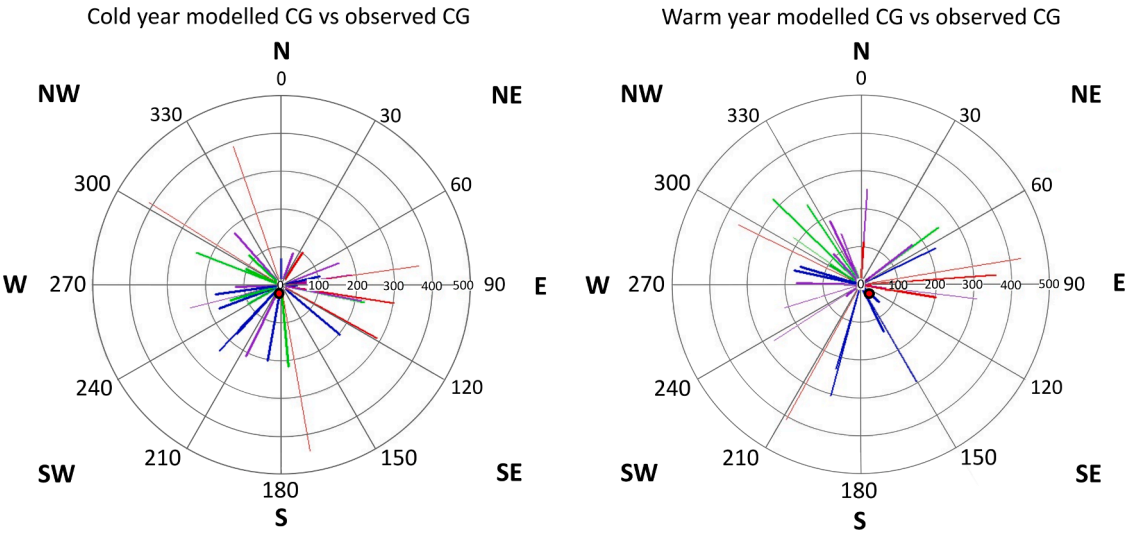

Fig. 7. Comparison of the distance and direction (azimuth) of difference in centre of gravity positions for functional groups in the Barents Sea Ecospace model. The distance and azimuth were calculated between the modelled (origo) centres of gravity and observed distribution centres of gravity. Each bar represents a functional group. Green lines represent the observed data with the lowest uncertainty score regarding the sampling; blue represents the second-lowest uncertainty; purple the third-lowest; and red the highest uncertainty score. The thickness of the lines represents the overlap index (GIC) between observed and modelled distribution; thinner lines represent low overlap while thick lines represent high overlap. The black-red spot represents the average position of the observed CGs of all compared FGs compared to the modelled CGs in the origo.

uncertainty score for the observed data, and CG differed significantly between uncertainty scores in the cold (KW, $\chi^2 = 8.83$, df = 3, $p = 0.03$) but not in the warm (KW, $\chi^2 = 1.92$, df = 3, $p = 0.58$) scenarios (**Appendix D** Figs. D1 and D2).

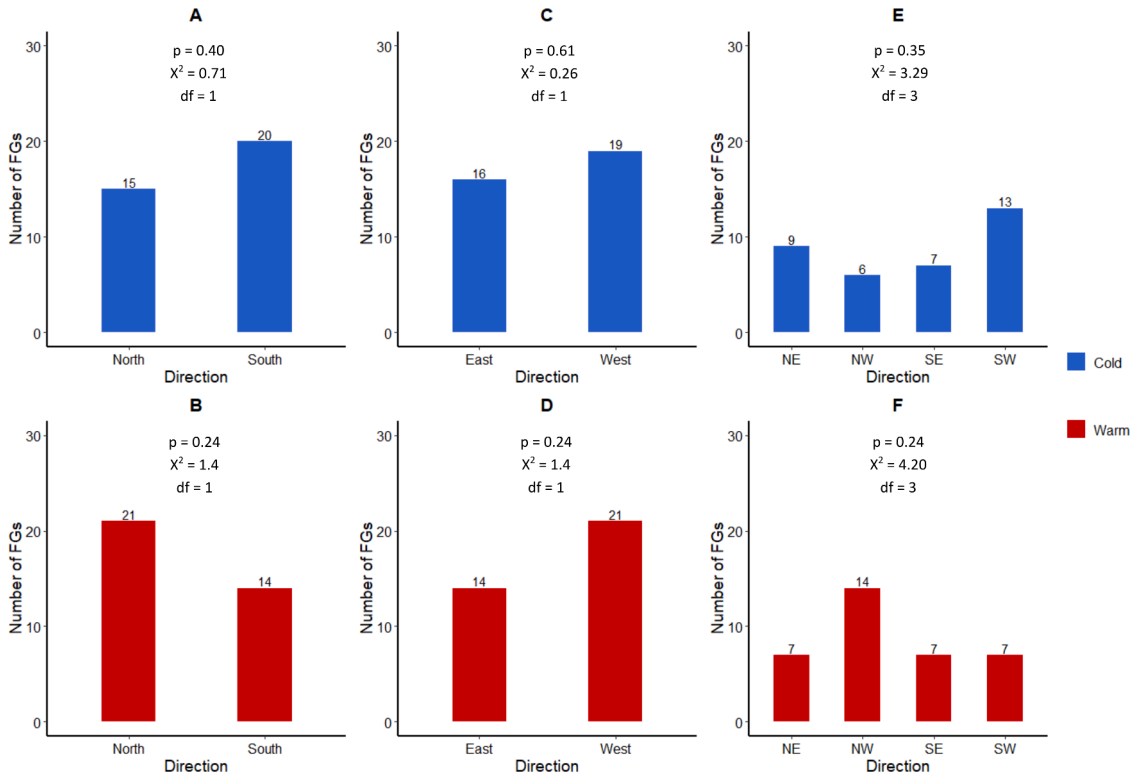

Fig. 8. Frequencies of directional shifts in distribution of CG for the FGs from modelled to observed distribution. Above are the chi-square values for test of equal number of FGs per direction category. (A) FGs with CG shifting when considering only northward and southward direction in cold years and (B) in warm year. (C) FGs with CG shifting when considering only eastward and westward direction in cold years and (D) in warm year. (F) FG with CG shifting when considering the four main directions in cold year and (F) in warm year.

3.2. Differences between distributions in cold and warm years

3.2.1. Differences between modelled distributions of FGs with lowest sampling uncertainties

Most FGs (80%) had more northerly CGs both from modelled and observed distributions in the warm than in the cold scenario ($\chi^2 = 25.20$, df = 1, $p < 0.001$ in both cases) (Table 3, Fig. 9). The north-south pattern of differences in CGs was similar in modelled and observed distributions (Figs. 9, 10) and the mean rate of poleward shift between 2004 and 2013 was 17 km year^{-1} for observed distributions and 7 km year^{-1} for the model outputs. The frequencies of northerly versus southerly differences for CGs between cold and warm scenarios did not significantly vary between modelled and observed distributions ($\chi^2 = 0.32$, df = 1, $p = 0.57$). The CGs from the modelled distributions showed a significant eastward shift from cold to warm years (86%, $\chi^2 = 17.86$, df = 1, $p < 0.001$). In contrast, the CGs from the observed distributions did not show a significant eastward shift from cold to warm years (57%, $\chi^2 = 0.71$, df = 1, $p = 0.40$) (Table 3, Fig. 9, Fig. 10). The average distances between CGs of cold and warm years were 56 km (SD 24) for the modelled, and 157 km (SD 80) for the observed distributions; the distributions of change in CGs differed significantly (KW$\chi^2 = 30.821$, df = 1, $p < 0.001$) (Table 3).

For the modelled distributions, 66% of the distribution CGs had a more north-easterly distribution in the warm than in the cold year, 20% a more south-easterly, and 14% a more north-westerly distribution ($\chi^2 = 33.91$, df = 3, $p < 0.01$) (Table 3, Fig. 9, Fig. 10). For observed distributions, 43% of CGs shifted towards the northeast from the cold to the warm year, 37% towards the northwest, 14% towards the southeast, and 6% towards the southwest ($\chi^2 = 13.34$, df = 3, $p < 0.01$) (Table 3, Fig. 9, Fig. 10). The most discrepant values were for large Greenland halibut with a distance of 345 km (azimuth 162°), saithe (age 0–2) with 237 km (azimuth 293°), and small herring with 198 km (azimuth 245°) (Table 3, Fig. 9).

For most FGs, the shifts in CG from cold to warm years were in the same direction for the modelled and observed distributions CGs (Table 3, Fig. 9). However, saithe age 3+, wolffishes, small herring, blue whiting, cephalopods, chaetognaths, small krill, and medium-sized copepods showed an utterly different bearing. Saithe age 0–2, large Greenland halibut, capelin age 0–2, and northern shrimps showed opposite directions of change in CGs from the cold to the warm year scenarios.

The average CG position of all 35 FGs for both modelled and observed distributions showed shifts from cold to warm years in a northeastward direction, towards 38° NE for the modelled and towards 12° NE for the observed distributions (Fig. 9). The distances in the shift of average values for CGs were also similar, with 41 km for the modelled and 68 km for the observed distributions (Fig. 9).

3.2.2. Differences between modelled distributions for all FGs

The Ecospace model shows poleward shifts in the distribution CG from cold to warm years for most FGs. Of the 104 non-detritus FGs included in this analysis, 83 FG shifted their distribution CG northerly and 21 FGs shifted their distribution CG southerly in the warm year scenario compared with the cold year scenario, including benthic and pelagic invertebrates. For more details, see **Appendix H**.

3.3. Predator-prey distribution overlap

The spatial overlap index between the main prey for the predators revealed that most prey of evaluated FGs had high spatial overlap with their predator distribution, both for modelled and observed distributions. However, the modelled predator FGs' distribution had significantly higher overlap (average GIC = 0.86, SD = 0.16) with their prey distribution than the observed distributions (GIC = 0.72, SD =0.18,

Table 3
Comparison of modelled and observed spatial distributions between the cold and the warm year scenarios. GIC is the global index of collocation between distributions of cold and warm years. Distance is the distance between the centre of gravity of the cold and warm years and angle is the angle between the centre of gravity from the cold to the warm years. Azimuth is the angle of the shift of the centre of gravity from cold (origo) to warm years, and bearing is the angle of the shift of the centre of gravity from cold (origo) to warm years in four quadrants of 90°

FG Number	FG Name	GIC		Distance (km)		Azimuth (degrees 360°)		Bearing (NE, SE, SW, NW)			
		modelled	observed	modelled	observed	modelled	observed	modelled		observed	
29	Northeast Arctic cod (3+)	1.00	0.84	34	287	22	353	22	NE	7	NW
33	Saithe (3+)	1.00	0.86	20	110	126	289	54	SE	71	NW
34	Saithe (0–2)	1.00	0.76	23	237	120	293	60	SE	67	NW
35	Haddock (3+)	0.98	0.91	89	181	111	23	69	SE	23	NE
36	Haddock (1–2)	0.98	0.94	78	125	111	23	49	SE	22	NE
37	Other small gadoids	1.00	0.98	4	35	114	92	66	SE	88	SE
38	Large Greenland halibut	1.00	0.75	24	345	8	162	8	NE	18	SE
39	Small Greenland halibut	0.99	1.00	64	5	340	322	20	NW	38	NW
41	Wolffishes	0.99	0.95	69	131	75	328	75	NE	32	NW
42	Stichaeidae	1.00	0.98	53	102	22	38	22	NE	38	NE
44	Other large bent invertebrate feeding fish	1.00	0.91	31	144	8	26	8	NE	26	NE
45	Thorny skate	0.99	0.96	80	131	66	84	66	NE	84	NE
46	Long rough dab	0.99	0.92	64	179	21	41	21	NE	41	NE
47	Other benthivore Flatfish	1.00	0.53	47	264	49	95	49	NE	65	NW
49	Small herring	1.00	0.78	14	198	72	245	72	NE	65	SW
50	Capelin age 3+	0.99	0.88	55	192	15	2	15	NE	2	NE
51	Capelin age 0–2	1.00	0.85	50	129	17	236	17	NE	56	SW
52	Polar cod age 2+	0.97	0.76	113	254	357	236	3	NW	15	NW
88	Blue whiting	0.99	0.93	55	85	92	339	88	SE	21	NW
57	Lumpfish	0.99	0.91	54	148	23	3	23	NE	3	NE
59	Large redfish	0.99	0.90	49	137	87	47	87	NE	47	NE
60	Small redfish	0.99	0.90	51	137	80	47	80	NE	47	NE
62	Cephalopods	0.98	1.00	89	28	344	104	16	NW	76	SE
63	Scyphomedusae	0.99	0.90	65	207	71	75	71	NE	75	NE
64	Chaetognaths	0.99	0.81	84	276	10	102	10	NE	78	SE
65	*Thysanoessa*	0.99	0.95	67	119	17	118	17	NE	62	SE
66	Large krill	0.99	0.77	56	257	102	89	78	SE	89	NE
71	Medium–sized copepods	0.99	0.92	65	149	78	293	78	NE	67	NW
79	Northern shrimp	0.99	1.00	58	28	38	218	38	NE	38	SW
80	Crangonid and other shrimps	0.99	0.92	86	171	6	24	6	NE	24	NE
81	Other large crustaceans	1.00	0.92	50	167	358	341	2	NW	19	NW
87	Predatory asteroids	1.00	0.95	35	81	356	47	4	NW	47	NE
91	Detrivorous polychaetes	1.00	0.96	56	78	27	342	27	NE	18	NW
82	Snow crab	0.99	0.83	79	148	7	45	7	NE	45	NE
	Average	0.99	0.88	56	157						
	SD	0.01	0.10	24	80						

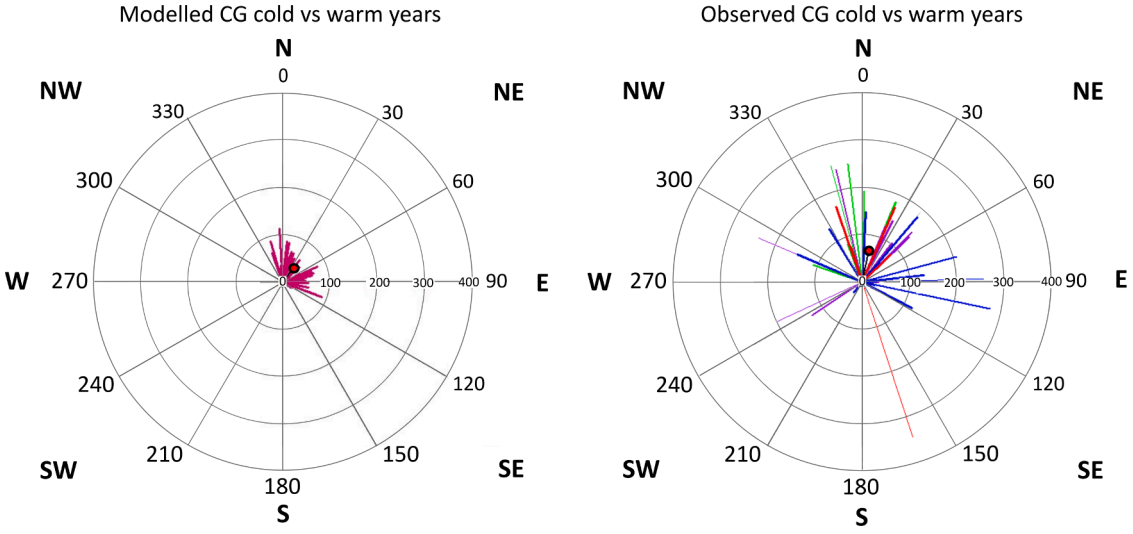

Fig. 9. Comparison of the difference in distance and azimuth of change in direction in centres of gravity for FGs between the cold and the warm year. The centre of gravity of the cold year distribution is at the centre of the plot. Each bar represents a functional group, and the centres of gravity for the warm year are positioned at the end of the bars. The thickness of the lines represents the overlap index (GIC) between cold and warm year distribution; thinner lines represent low overlap while thicker represent high overlap. The black and red spot represents the average centre of gravity shift from cold to warm years. In the observed figure, green lines represent the observed data with the lowest uncertainty score regarding the sampling; blue represent the second-lowest; purple the third-lowest; and red the highest uncertainty score.

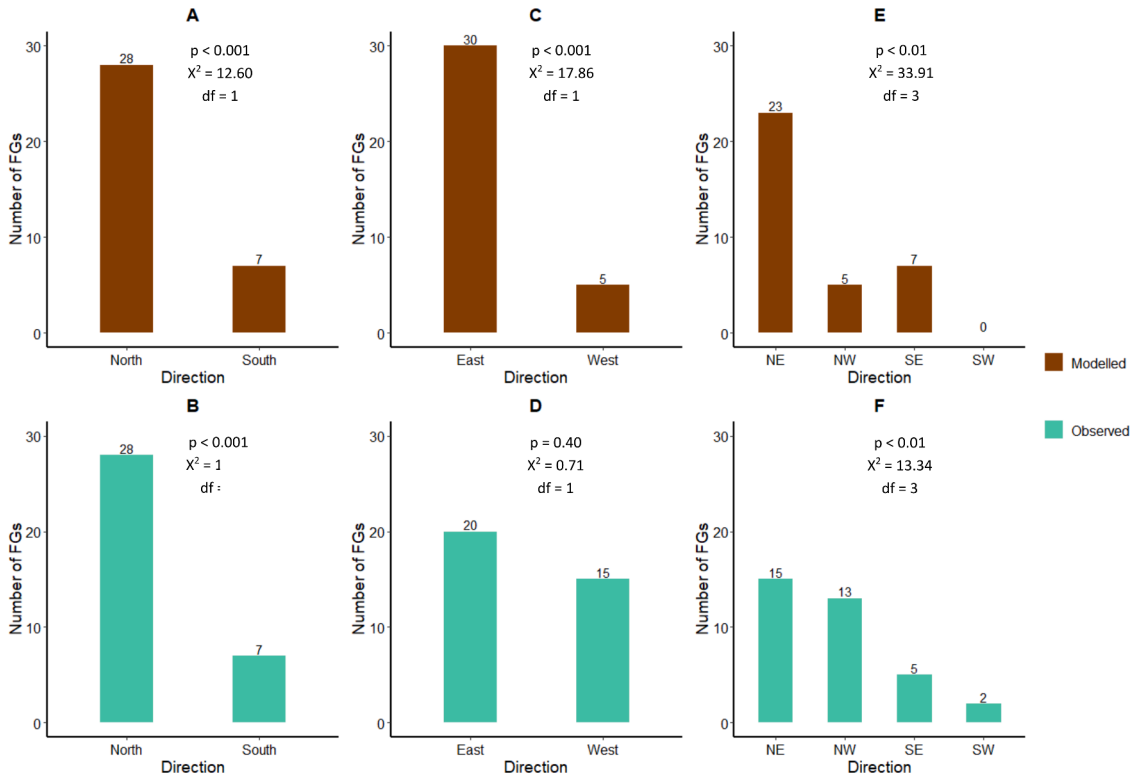

Fig. 10. Frequencies of directional shifts in the distribution of CG for the FGs from cold to warm years. Above are the chi-square values, p-values, and df for the test of an equal number of FGs per direction category. (A) FGs with CG shifting when considering only northward and southward direction in the modelled and (B) in observed distributions. (C) FGs with CG shifting when considering only eastward and westward direction in the modelled and (D) in observed distributions. (E) FG with CG shifting when considering the four main directions in the modelled and (F) in the observed distributions.

Appendix D, Table D3) (Paired T-test $t = 5.51$, df $= 42$, $p<0.05$).

3.4. Changes in the Barents Sea community distribution in the last decade due to warming conditions

The average CG position of all 104 living modelled FGs, excluding the detritus groups, shifted 40 km poleward from 2004 to 2013 on a

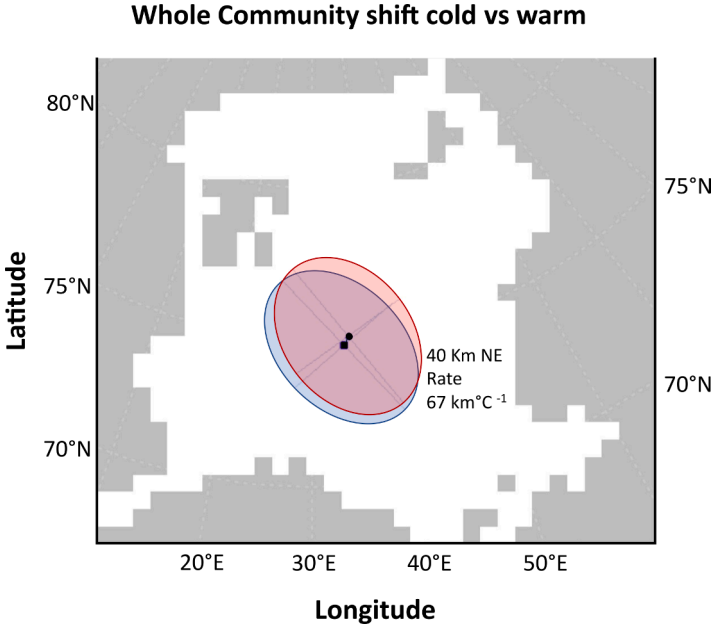

Fig. 11. Average CG position and inertia area of all modelled FGs. The centre of the cross is the average position of the CG for the whole community, the square is the cold year, and the circle is the warm year. The ellipses represent the average inertia for all 104 FGs: the blue is the cold year and the red is the warm year. The distance between the two CGs and the average rate is shown to the right of the ellipses.

bearing of 27° NE Fig. 11 and **Appendix H**). Based on the average CGs for 2004 and 2013 and the nine years' time interval, the community shifted poleward at a rate of 4.4 km year^{-1}. The rate of the poleward shift of the whole community was 67 km °C^{-1} based on the surface water temperature and 133 km °C^{-1} based on the bottom water temperature.

3.5. Changes in the distribution area with warming

The average inertia area was 275,302 km^2 (sd = 103,982) in the cold year (2004) and 286,802 km^2 (sd = 106,737) in the warm year, corresponding to an increase of 4%. The inertia areas of all modelled FGs were significantly larger in warm than in cold years (paired Wilcoxon test, $V = 725$, $p < 0.001$). Based on the Aquamaps thermal limits of the species, 17% of the FGs are **arctic**, 14% **arctic-boreal**, 51% **boreal**, and 17% **broad**. Most FG groups increased the inertia in warmer conditions (73%), 22% reduced, and 5% neither increased nor decreased. All **broad** FGs increased the inertia area in warmer conditions, though a few FGs reduced the inertia area in all other biogeographical categories. Of all 23 FGs that reduced the inertia area in warmer conditions, only six reduced the inertia area by more than 5% in warmer conditions. Large calanoids was the FG with the most considerable reduction in inertia area in warmer conditions (−11%), followed by bowhead (−7%, thermal range = 4.8 °C), narwhale (−6%, thermal range = 12.7 °C), and other piscivorous fish (−6%, thermal range = 8.1 °C). Within the FGs that increased inertia area in warmer conditions, the difference was larger, with the symphagic amphipods being the FG with the most considerable difference (+63%) followed by mackerel (+42%, thermal range = 11.8 °C), and sperm whale (+27%, thermal range = 16 °C); for all the other 73 FGs with larger inertia area in warmer conditions, the increment ranged between +1 and +22 °C (**Appendix D**, Fig. D3). However, they do not differ significantly amongst the biogeographical groups (Kruskal Wallis test KW = 0.7, df = 3, $p = 0.86$).

4. Discussion

4.1. Evaluation of the Ecospace model

As far as we know, this is the first spatial model for the Barents Sea at the food web level, comprising FGs at all trophic levels and with the same spatial resolution as the survey field-observed spatial distributions. Our study shows that the Ecospace modelled and observed spatial distributions can easily be compared and evaluated by using CG and inertia.

It is known that the species distributions in the Barents Sea are strongly related to the environmental conditions (Aune et al., 2021; Dalpadado et al., 2003; Loeng, 1989b; Nakken and Raknes, 1987). The ability to predict these distributions in the context of environmental changes and differential natural resource usage can be very beneficial for resource management and species conservation. The Ecospace model includes multiple spatial drivers that are coupled to the foraging capacity of FGs. This enable Ecospace to simulate spatial responses to multiple physical, oceanographic, and environmental drivers (Christensen et al., 2014; Coll et al., 2019), and contribute to a good representation of the FGs distribution with a high overlap between the observed and modelled distribution.

During the process of individual inclusion of the habitat capacities and comparison with the survey-observed distribution, we observed that depth, bottom, and surface temperatures were crucial to model the species' distributions in the Barents Sea Ecospace model. This is in line with other studies that identified these environmental drivers as good predictors of species distributions in the Barents Sea (Husson et al., 2020) as well in other marine ecosystems (Burgos et al., 2020; Coll et al., 2019).The use of the habitat foraging capacity functions, and contrasting warm and relatively colder years, allowed us to observe the relevance of the inclusion of temperature, depth, ice, and productivity as forcings to predictive models, as they proved to be essential to describe the changes observed between cold and warm years in the Barents Sea LME. The use of habitat capacities based on the QGAM method for Barents Sea data improved the fit of the model to observed distributions. However, information from literature (e.g., Aquamaps, Fishbase and SeaLifeBase), similar to what we used for species with no local information for habitat capacity, has been used exclusively or as complementary to distribution descriptor tools in many studies (e.g., Adebola and de Mutsert, 2019; Coll et al., 2019, 2020). Coll et al. (2019) argued that the modelling tools used to describe species distributions, such as QGAM, can be complemented by either using the response functions derived from statistical analysis in the Ecopath calculations or by forcing the niche priors of Ecospace foraging capacity directly with the results from the statistical model. Using the foraging habitat capacity is crucial for more reliable results, as we were able to confirm in our model. Ecospace is a dynamic model that includes predator-prey interactions and, in our study, the use of habitat capacity functions to force distributions leds to more realistic spatial distributions for some FGs that lacked habitat capacities. When there was no information available locally, e.g., based on field data for the Ecospace model area, sources such as FishBase and SeaLifeBase were useful to derive habitat foraging capacity functions.

Trophic models always carry some uncertainties, generalisations, and different levels of accuracy in the data and the FG. In a model as large as the present Ecospace model, some FGs consist of several species while others represent single species (**see Appendix F)**. However, we argue that the model can effectively predict the spatial distributions for all evaluated FGs.

The FGs with assumed high uncertainty in field-sampled distributions were expected to overlap less with the model output than the FGs with assumed low uncertainty. This can be observed with Greenland halibut FGs categorised as having a high uncertainty of sampling (score 4). According to the Ecosystem Survey report (Anon., 2004), large Greenland halibut distribution was primarily outside of the survey area in the Ecosystem Survey in 2004. This could affect both the small and large Greenland halibut observed distribution. The same report discusses how adult Greenland halibut's main concentrations were in the deeper part of the Spitsbergen slope and southeast of a line drawn between Bear Island and Hopen Island (Anon., 2004), close to where our model shows the centre of gravity of this species' distribution. It suggests that, despite the lower overlap index value for this species, our model may represent the distribution close to the expected natural distribution of this species. In the warm year (2013), the observed and modelled distributions of both FGs of Greenland halibut overlapped more than in the cold year (2004). This could reflect the enlargement of the sampled area northeast of the original area in 2013 (Prokhorova, 2013).

None of the Ecosystem Surveys covered the extreme northeastern part of the study area (Eriksen, 2014). Thus, because of incomplete coverage in this area, the spatial distributions for some FGs from the Ecosystem Survey could show more southerly distributions than the real distributions. The Barents Sea is deepest in the southwest, where the bottom water is warmest (Loeng and Drinkwater, 2007). Thus, a northward change in the distribution of a species will also affect its depth distribution, affecting predator-prey relationships and potentially affecting predation mortalities and competition effects (Fall et al., 2018). The generally higher overlap for modelled than observed predator-prey may result from the inability of the model to incorporate all the complexity of the natural systems, in which FGs can make new and unexpected connections in response to restrictions or lack of resources that the model cannot predict.

4.2. Changes in modelled and observed distributions between cold and warm years

That the observed distributions were positioned more northerly in warm than in cold years was expected for high-latitude species in warmer conditions (Eriksen et al., 2017; Fossheim et al., 2015; Frainer

et al., 2017; Poloczanska et al., 2016; Skaret et al., 2014). The model outputs showed a similar northeastward shift from the cold to the warm scenario, indicating that our model may be a good predictor tool for the effects of warming on spatial distribution changes of functional groups in the Barents Sea ecosystem. This distribution shift was expected and is in line with other model predictions of changes in species distributions due to global warming, showing boreal and arctic species moving their distributions poleward, albeit in different ways (Christiansen et al., 2014; Fossheim et al., 2015; Frainer et al., 2017; Hollowed et al., 2013; Perry et al., 2005; Poloczanska et al., 2016; Pörtner and Gutt, 2016).

The similar average CG position of the modelled and the observed FGs' distributions in cold and warm years indicates a similar average distribution pattern in the modelled and observed data. The poleward shifts from the cold to warm years in average CG were similar for the modelled (41 km) and observed (68 km) data and could indicate a similar average response to change in temperature in modelled and observed distributions. However, some FGs have shown different bearings in the shift between cold and warm years, though most displacements were in similar directions to what was observed by field surveys. Thus, we can affirm that our model can effectively and spatially represent the Barents Sea ecosystem and its past changes due to environmental changes.

4.3. Effects of warming on distribution of the whole community

Most (80%) of the 104 living FGs of the model shifted distribution poleward in the warm scenario. The other groups (e.g., coastal cod, saithe, and other small gadoids) mostly shifted distribution southeastward, which may to some extent also be a result of a search for colder conditions. This is because the southeastern part of the Barents Sea LME is colder than the western part, mainly due to the contact with the White and Kara seas, known for being cold seas (Kohnemann et al., 2017). We included 'distance off the coast' as habitat capacity for some FGs that shifted distribution towards the southeast, and this restricted the FGs from moving to colder conditions in the northern Barents Sea, 'forcing' these FGs to move to cold conditions in the southeastern Barents Sea. Some boreal species associated with the warmer Atlantic water, such as mackerel, Atlantic puffin, and blue whiting, shifted their distribution towards the southwest. In these cases, when evaluating their natural distributions (Anker-Nilssen et al. 2000; Belikov et al. 2011; Olafsdottir et al., 2019), this shift direction means that they are expanding into the Barents Sea, probably already due to the Atlantification of the Barents Sea with the warming conditions of the past few decades.

The rate of poleward shift based on average CGs of all the modelled FGs in our study was 4.4 km year^{-1} between the 2004 and 2013 scenarios. This community shift rate seems to be higher than most poleward shifts of organisms due to warming reported in other studies. In the North Sea, six demersal fish species moved north (boundaries of the distribution) at a rate of 2.2 km year^{-1} in warmer conditions (Perry et al., 2005). In Iceland's coastal waters, 82 fish species showed distribution shifts at a mean rate of 0.014° latitude/year (~1.55 km year^{-1}), most of them poleward, during 22 years with warming conditions (Campana et al., 2020).

The shift rate of the centre of distribution produced by our model seems to be similar to rates observed in other subpolar and boreal areas. In our study, the community as a whole shifted on average 67 km °C^{-1} poleward based on the surface temperature although, based on the bottom temperature, the community as a whole shifted 133 km °C^{-1} poleward. Campana et al. (2020) observed an average shift of 38 km °C^{-1} in the fish community distribution in Icelandic waters based on average water column temperature. In the North Sea, Dulvy et al. (2008) observed a poleward shift of demersal fish species at a rate that ranged between 10 and 70 km °C^{-1} based on temperature from the lower half of the water column, and Perry et al. (2005) observed an average distribution shift of 164 km °C^{-1} for 15 demersal fishes based on bottom temperature.

The measures for water temperature may be critical for the value of shift rate because surface waters are more susceptible to rises in air temperature while deeper waters are more thermally stable (Manabe et al., 1990). Thus, the shift rate based on bottom temperature tends to be higher than based on surface or the whole water column temperature. Our study shows results similar to those which Perry et al. (2005) found in the North Sea. The shift rate in our study was based on the average CG position for the whole community, including benthic and pelagic species, and steno- and eurythermal species. The rate can vary depending on the FG and their particularities, and here our point is to present an overview of the community pattern in the Barents Sea.

4.4. Thermal responses to warming

Boreal and arctic species in the Barents Sea differ markedly regarding resource use and habitat affinities, and how environmental changes impact their distribution and the community as a whole (Frainer et al., 2017). Many authors have argued that boreal species have tended to move or increase their distributions poleward during the period of recent warming (Fossheim et al., 2015; Perry et al., 2005; Poloczanska et al., 2016). In contrast, arctic species have been observed to reduce the area of their distributions by being restricted to high latitudes, searching for polar conditions (Christiansen et al., 2014; Fossheim et al., 2015; Frainer et al., 2017; Hollowed et al., 2013; Pörtner and Gutt, 2016). In our study, a few FGs reduced their modelled distribution areas under warmer conditions. On average, even the stenothermal arctic and arctic-boreal FGs more frequently increased than reduced distribution areas in warmer conditions. Campana et al. (2020) argued that in Iceland, the stenothermal species with a distribution close to their thermal limits were the most likely to change their distribution. The increase in the water temperature observed in the Barents Sea in the period of the present study was probably too small to force the water temperature close to the thermal limit of any stenothermal species in the Barents Sea. This may be one possible explanation for the overall increase in the distribution area in warmer conditions in our study.

4.5. Limitations of the study

Some of the observed distributions were not from 2004, which represented a cold year, or from 2013, which represented a warm year, but were from other years with different environmental conditions that may have contributed to less accurate results. It is evident that once we were not constantly comparing the same years (and consequently not the same environmental conditions), we could not include all relevant environmental and physiological possible variables. Thus, we did not expect a complete distribution overlap between observed and modelled functional groups. However, the generally high spatial overlap between observed and modelled distribution indicates the good representativity of our model. Even though the Barents Sea Ecospace model has some limitations, it seems to effectively model the spatial distributions of FGs in the Barents Sea LME well.

5. Conclusions

The Ecospace model of the Barents Sea LME simulated similar spatial distributions of FGs as did the survey-based observed distributions in cold and warm years. Most FGs shifted their modelled and observed distributions poleward under warmer conditions. The poleward shifts in the average centre of gravity for the 35 FGs with observational data was 41 km for modelled and 68 km for observed distributions. The whole modelled community shifted 40 km towards the northeast (poleward) from the relatively cold 2004 to the warm 2013, corresponding to a shift rate of 67 km °C^{-1} surface temperature and 133 km °C^{-1} bottom temperature. The warming conditions led to an average increase of 4% in the modelled FGs distribution area measured as inertia area. The Ecopspace model for the Barents Sea can be used to predict future

changes in spatial distributions under warming scenarios. We are now using the model applying different climatic scenarios and spatio-temporal predictions, to answer questions regarding the impacts of fishery and global changes on future mid- and long-term scenarios.

CRediT authorship contribution statement

Marcela C. Nascimento: Conceptualization, Data curation, Formal analysis, Writing – original draft, Writing – review & editing. **Berengere Husson:** Data curation, Formal analysis, Writing – review & editing. **Lilia Guillet:** Data curation, Writing – review & editing. **Torstein Pedersen:** Conceptualization, Data curation, Formal analysis, Writing – review & editing, Project administration, Supervision.

Declaration of Competing Interest

The authors declare that they have no known competing financial interests or personal relationships that could have appeared to influence the work reported in this paper.

Data availability

Data input and all maps are available online in the Supplementary material

Acknowledgments

We wish to thank the Nansen Legacy Project for financial support, Micael Eiji Nagai for support with R codes, Rod Wolstenholme for the adaptation of the study area map, and Mikko Vihtakari for the use of R package ggOceanMaps to plot the Barents Sea map.

Funding

The Research Council of Norway provided support through the Nansen Legacy Project (RCN#276730).

Supplementary materials

Supplementary material associated with this article can be found, in the online version, at doi:10.1016/j.ecolmodel.2023.110358.

References

Adebola, T., de Mutsert, K., 2019. Spatial simulation of redistribution of fishing effort in Nigerian coastal waters using Ecospace. Ecosphere 10, e02623. 10.1002/ecs2.2623.

Ahrens, R.N.M., Walters, C.J., Christensen, V., 2012. Foraging arena theory. Fish Fish. 13, 41–59. https://doi.org/10.1111/j.1467-2979.2011.00432.x.

Andriyashev, A., Chernova, N., 1995. Annotated list of fishlike vertebrates and fish of the Arctic seas and adjacent waters. J. Ichthyol./Vopr. Ikhtiol. 35, 4.

Anon., 2004. Survey report from the Joint Norwegian/Russian ecosystem survey in the Barents Sea August-October 2004. Institute of Marine Research (IMR) and Polar Research Institute of Marine Fisheries and Oceanography (PINRO) 68 pp.

Anker-Nilssen, T., Bakken, V., Strøm, H., Golovkin, A.N., Bianki, V.V., Tatarinkova, I.P., 2000. The status of marine birds breeding in the Barents Sea region. Norwegian Polar Institute Report Serie 113–2000.

Audzijonyte, A., Pethybridge, H., Porobic, J., Gorton, R., Kaplan, I., Fulton, E.A., 2019. Atlantis: a spatially explicit end-to-end marine ecosystem model with dynamically integrated physics, ecology and socio-economic modules. Methods Ecol. Evol. 10, 1814–1819. https://doi.org/10.1111/2041-210X.13272.

Aune, M., Raskhozheva, E., Andrade, H., Augustine, S., Bambulyak, A., Camus, L., Carroll, J., Dolgov, A.V., Hop, H., Moiseev, D., Renaud, P.E., Varpe, Ø., 2021. Distribution and ecology of polar cod (Boreogadus saida) in the eastern Barents Sea: a review of historical literature. Mar. Environ. Res. 166, 105262 https://doi.org/10.1016/j.marenvres.2021.105262.

Belikov, S.V., Oganin, I.A., Høines, Å., 2011. Blue whiting. In: Jakobsen, T., Ozhigin, V.K. (Eds.), The Barents Sea Ecosystem, Resources and Management. Tapir Academic Press, Trondheim, pp. 37–76.

Buhl-Mortensen, L., Buhl-Mortensen, P., Dolan, M.F.J., Holte, B., 2015. The MAREANO programme—a full coverage mapping of the Norwegian offshore benthic environment and fauna. Mar. Biol. Res. 11, 4–17. https://doi.org/10.1080/17451000.2014.952312.

Burgos, J.M., Buhl-Mortensen, L., Buhl-Mortensen, P., Ólafsdóttir, S.H., Steingrund, P., Ragnarsson, S.Á., Skagseth, Ø., 2020. Predicting the distribution of indicator taxa of vulnerable marine ecosystems in the Arctic and Sub-arctic waters of the Nordic Seas. Front. Mar. Sci. 7, 131. https://doi.org/10.3389/fmars.2020.00131.

Cade, B.S., Noon, B.R., Flather, C.H., 2005. Quantile regression reveals hidden bias and uncertainty in habitat models. Ecology 86, 786–800. https://doi.org/10.1890/04-0785.

Campana, S.E., Stefánsdóttir, R.B., Jakobsdóttir, K., Sólmundsson, J., 2020. Shifting fish distributions in warming sub-Arctic oceans. Sci. Rep. 10, 16448. https://doi.org/10.1038/s41598-020-73444-y.

Charles, S., Kooperberg, L., Ripley, R., Ripley, M., 2002. The logspline Package.

Christensen, V., Coll, M., Steenbeek, J., Buszowski, J., Chagaris, D., Walters, C.J., 2014. Representing variable habitat quality in a spatial food web model. Ecosystems 17, 1397–1412. https://doi.org/10.1007/s10021-014-9803-3.

Christensen, V., Pauly, D., 1992. ECOPATH II—a software for balancing steady-state ecosystem models and calculating network characteristics. Ecol. Model. 61, 169–185. https://doi.org/10.1016/0304-3800(92)90016-8.

Christensen, V., Walters, C., Pauly, D., Forrest, R., 2008. Ecopath With Ecosim Version 6. User Guide. Fisheries Centre. University of British Columbia, Vancouver.

Christensen, V., Walters, C.J., 2004. Ecopath with Ecosim: methods, capabilities and limitations. Ecol. Model. 172, 109–139. https://doi.org/10.1016/j.ecolmodel.2003.09.003.

Christiansen, J.S., Mecklenburg, C.W., Karamushko, O.V., 2014. Arctic marine fishes and their fisheries in light of global change. Global Change Biol. 20, 352–359. https://doi.org/10.1111/gcb.12395.

Coll, M., Pennino, M.G., Steenbeek, J., Sole, J., Bellido, J.M., 2019. Predicting marine species distributions: complementarity of food-web and Bayesian hierarchical modelling approaches. Ecol. Model. 405, 86–101. https://doi.org/10.1016/j.ecolmodel.2019.05.005.

Coll, M., Steenbeek, J., Pennino, M.G., Buszowski, J., Kaschner, K., Lotze, H.K., Rousseau, Y., Tittensor, D.P., Walters, C., Watson, R.A., Christensen, V., 2020. Advancing global ecological modeling capabilities to simulate future trajectories of change in marine ecosystems. Front. Mar. Sci. 7 https://doi.org/10.3389/fmars.2020.567877.

Cribari-Neto, F., Zeileis, A., 2010. Beta regression in R. J. Stat. Softw. 34, 1–24. https://doi.org/10.18637/jss.v034.i02.

Dalpadado, P., Arrigo, K.R., van Dijken, G.L., Skjoldal, H.R., Bagøien, E., Dolgov, A., Prokopchuk, I., Sperfeld, E., 2020. Climate effects on temporal and spatial dynamics of phytoplankton and zooplankton in the Barents Sea. Prog. Oceanogr. 102320 https://doi.org/10.1016/j.pocean.2020.102320.

Dalpadado, P., Ingvaldsen, R., Hassel, A., 2003. Zooplankton biomass variation in relation to climatic conditions in the Barents Sea. Polar Biol. 26, 233–241. https://doi.org/10.1007/s00300-002-0470-z.

Delignette-Muller, M.L., Dutang, C., 2015. fitdistrplus: an R package for fitting distributions. J. Stat. Softw. 64, 1–34. https://doi.org/10.18637/jss.v064.i04.

Dolgov, A., 2016. Composition, Formation and Trophic Structure of the Barents Sea Fish Communities. PINRO, Murmansk (In Russian), p. 336.

Drinkwater, K.F., 2011. The influence of climate variability and change on the ecosystems of the Barents Sea and adjacent waters: review and synthesis of recent studies from the NESSAS Project. Prog. Oceanogr. 90, 47–61. https://doi.org/10.1016/j.pocean.2011.02.006.

Dulvy, N.K., Rogers, S.I., Jennings, S., Stelzenmüller, V., Dye, S.R., Skjoldal, H.R., 2008. Climate change and deepening of the North Sea fish assemblage: a biotic indicator of warming seas. J. Appl. Ecol. 45, 1029–1039. https://doi.org/10.1111/j.1365-2664.2008.01488.x.

Eriksen, E. (ed.) 2014. Survey report from the joint Norwegian/Russian ecosystem survey in the Barents Sea and adjacent waters, August-October 2014 153 pp. 10.13140/RG.2.2.34304.69124.

Eriksen, E., Dalpadado, P., 2011. Long-term changes in Krill biomass and distribution in the Barents Sea: are the changes mainly related to capelin stock size and temperature conditions? Polar Biol. 34, 1399–1409. https://doi.org/10.1007/s00300-011-0995-0.

Eriksen, E., Gjøsæter, H., Prozorkevich, D., Shamray, E., Dolgov, A., Skern-Mauritzen, M., Stiansen, J.E., Kovalev, Y., Sunnanå, K., 2018. From single species surveys towards monitoring of the Barents Sea ecosystem. Prog. Oceanogr. 166, 4–14. https://doi.org/10.1016/j.pocean.2017.09.007.

Eriksen, E., Skjoldal, H.R., Gjøsæter, H., Primicerio, R., 2017. Spatial and temporal changes in the Barents Sea pelagic compartment during the recent warming. Prog. Oceanogr. 151, 206–226. https://doi.org/10.1016/j.pocean.2016.12.009.

Fall, J., Ciannelli, L., Skaret, G., Johannesen, E., 2018. Seasonal dynamics of spatial distributions and overlap between Northeast Arctic cod (Gadus morhua) and capelin (Mallotus villosus) in the Barents Sea. PLoS One 13, e0205921. https://doi.org/10.1371/journal.pone.0205921.

Fasiolo, M., Goude, Y., Nedellec, R., Wood, S., 2017. Fast calibrated additive quantile regression. J. Am. Stat. Assoc. 116 https://doi.org/10.1080/01621459.2020.1725521.

Fossheim, M., Primicerio, R., Johannesen, E., Ingvaldsen, R.B., Aschan, M.M., Dolgov, A.V., 2015. Recent warming leads to a rapid borealization of fish communities in the Arctic. Nat. Clim. Change 5, 673–677. https://doi.org/10.1038/nclimate2647.

Frainer, A., Primicerio, R., Kortsch, S., Aune, M., Dolgov, A.V., Fossheim, M., Aschan, M.M., 2017. Climate-driven changes in functional biogeography of Arctic marine fish communities. Proc. Natl. Acad. Sci. U. S. A. 114, 12202–12207. https://doi.org/10.1073/pnas.1706080114.

Fulton, E.A., Bulman, C.M., Pethybridge, H., Goldsworthy, S.D., 2018. Modelling the Great Australian Bight ecosystem. Deep Sea Res. 157-158, 211–235. https://doi.org/10.1016/j.dsr2.2018.11.002 (II Top. Stud. Oceanogr.).
Gonzalez-Mirelis, G., Ross, R.E., Albretsen, J., Buhl-Mortensen, P., 2021. Modeling the distribution of habitat-forming, deep-sea sponges in the Barents Sea: the value of data. Front. Mar. Sci. 7 https://doi.org/10.3389/fmars.2020.496688.
González-Pola, C., Larsen, K.M.H., Fratantoni, P., Beszczynska-Möller, A. (eds.) 2020. ICES Report on Ocean Climate 2019 136 pp. 10.17895/ices.pub.7537.
Hayford, J.F., 1909. Geodesy: the Figure of the Earth and Isostasy from Measurements in the United States US Government Printing Office 178 pp.
Hollowed, A.B., Planque, B., Loeng, H., 2013. Potential movement of fish and shellfish stocks from the sub-Arctic to the Arctic Ocean. Fish. Oceanogr. 22, 355–370. https://doi.org/10.1111/fog.12027.
Hunt, G.L., Blanchard, A.L., Boveng, P., Dalpadado, P., Drinkwater, K.F., Eisner, L., Hopcroft, R.R., Kovacs, K.M., Norcross, B.L., Renaud, P., 2013. The Barents and Chukchi Seas: comparison of two Arctic shelf ecosystems. J. Mar. Syst. 109, 43–68. https://doi.org/10.1016/j.jmarsys.2012.08.003.
Huse, G., Ellingsen, I., 2008. Capelin migrations and climate change—a modelling analysis. Clim. Change 87, 177–197. https://doi.org/10.1007/s10584-007-9347-z.
Huse, G., Johansen, G.O., Bogstad, B., Gjøsæter, H., 2004. Studying spatial and trophic interactions between capelin and cod using individual-based modelling. ICES J. Mar. Sci. 61, 1201–1213. https://doi.org/10.1016/j.icesjms.2004.06.011.
Husson, B., Certain, G., Filin, A., Planque, B., 2020. Suitable habitats of fish species in the Barents Sea. Fish. Oceanogr. 29, 526–540. https://doi.org/10.1111/fog.12493.
Ingvaldsen, R.B., Assmann, K.M., Primicerio, R., Fossheim, M., Polyakov, I.V., Dolgov, A. V., 2021. Physical manifestations and ecological implications of Arctic Atlantification. Nat. Rev. Earth Environ. https://doi.org/10.1038/s43017-021-00228-x.
Jørgensen, L.L., Ljubin, P., Skjoldal, H.R., Ingvaldsen, R.B., Anisimova, N., Manushin, I., 2015. Distribution of benthic megafauna in the Barents Sea: baseline for an ecosystem approach to management. ICES J. Mar. Sci. 72, 595–613. https://doi.org/10.1093/icesjms/fsu106.
Jørgensen, S.E., Fath, B.D., 2011. Fundamentals of Ecological Modelling: Applications in Environmental Management and Research, fourth ed. Elsevier.
Kaschner, K., Kesner-Reyes, K., Garilao, C., Segschneider, J., Rius-Barile, J. Rees, T., Froese, R. 2019. AquaMaps: predicted range maps for aquatic species. Retrieved from https://www.aquamaps.org. (accessed 15 November 2022).
Kleisner, K.M., Fogarty, M.J., McGee, S., Hare, J.A., Moret, S., Perretti, C.T., Saba, V.S., 2017. Marine species distribution shifts on the U.S. Northeast Continental Shelf under continued ocean warming. Prog. Oceanogr. 153, 24–36. https://doi.org/10.1016/j.pocean.2017.04.001.
Kohnemann, S.H.E., Heinemann, G., Bromwich, D.H., Gutjahr, O., 2017. Extreme warming in the Kara Sea and Barents Sea during the Winter Period 2000–16. J. Clim. 30, 8913–8927. https://doi.org/10.1175/jcli-d-16-0693.1.
Lien, V., Gusdal, Y., Albretsen, J., Melsom, A., Vikebø, F., 2013. Evaluation of a Nordic Seas 4km numerical ocean model hindcast archive (SVIM), 1960-2011. Fisk. Havet 7, 1–80.
Loeng, H., 1989a. Ecological Features of the Barents Sea, in: Rey, L., Alexander, V. (Eds.), Proceedings of the 6th of the Comit.. Arctique International. EJ Brill, Leiden, The Netherlands.
Loeng, H., 1989b. The influence of temperature on some fish population parameters in the Barents Sea. J. Northwest Atl. Fish. Sci. 9 https://doi.org/10.2960/J.v9.a9.
Loeng, H., 1991. Features of the physical oceanographic conditions of the Barents Sea. Polar Res. 10 (1), 5–18. https://doi.org/10.3402/polar.v10i1.6723.
Loeng, H., Drinkwater, K., 2007. An overview of the ecosystems of the Barents and Norwegian Seas and their response to climate variability. Deep Sea Res. 54, 2478–2500. https://doi.org/10.1016/j.dsr2.2007.08.013 (II Top. Stud. Oceanogr.).
Mackinson, S., Daskalov, G., 2007. An ecosystem model of the North Sea to support an ecosystem approach to fisheries management: description and parameterisation. Sci. Ser. Tech Rep. Cefas Lowestoft 142, 196pp.
Manabe, S., Bryan, K., Spelman, M.J., 1990. Transient response of a global ocean-atmosphere model to a doubling of atmospheric carbon dioxide. J. Phys. Oceanogr. 20 (5), 722–749. https://doi.org/10.1175/1520-0485(1990)020<0722:TROAGO>2.0.CO;2.
Marine regions, 2022. https://www.marineregions.org/gazetteer.php?p=details&id=8526/ (aceessed 13 November 2022).
Mikhina, A., Draganova, E., Kanishcheva, O., Evseeva, E., Zaytseva, K., 2019. Dynamics of macro-plankton communities of the Barents Sea, in: E. Shamray, G. Huse, A. Trofimov, S. Sundby, A. Dolgov, H. R. Skjoldal et al., A. Filin, T. Haug, Zabavnikov, V. (Eds.), Influence of Ecosystem Changes on Harvestable Resources at High Latitudes. The Proceedings of the 18th Russian-Norwegian Symposium,Murmansk, Murmansk, Russia.
Nakken, O., Raknes, A., 1987. The distribution and growth of Northeast Arctic cod in relation to bottom temperatures in the Barents Sea, 1978–1984. Fish. Res. 5, 243–252. https://doi.org/10.1016/0165-7836(87)90044-0.
Nordøy, E.S., Folkow, L.P., Potelov, V., Prischemikhin, V., Blix, A.S., 2008. Seasonal distribution and dive behaviour of harp seals (*Pagophilus groenlandicus*) of the White Sea–Barents Sea stock. Polar Biol. 31, 1119. https://doi.org/10.1007/s00300-008-0453-9.
Olafsdottir, A.H., Utne, K.R., Jacobsen, J.A., Jansen, T., Óskarsson, G.J., Nøttestad, L., Elvarsson, B.Þ., Broms, C., Slotte, A., 2019. Geographical expansion of Northeast Atlantic mackerel (Scomber scombrus) in the Nordic Seas from 2007 to 2016 was primarily driven by stock size and constrained by low temperatures. Deep Sea Res. II 159, 152–168. https://doi.org/10.1016/j.dsr2.2018.05.023.
Orlova, E.L., Rudneva, G.B., Renaud, P.E., Eiane, K., Savinov, V., Yurko, A.S., 2010. Climate impacts on feeding and condition of capelin Mallotus villosus in the Barents Sea: evidence and mechanisms from a 30 year data set. Aquat. Biol. 10, 105–118. https://doi.org/10.3354/ab00265.
Ozhign, V.K., Ingvaldsen, R.B., Loeng, H., Boitsov, V.D., Karsakov, A.L., 2011. The Barents Sea. In: Jakobsen, T., Ozhigin, V.K. (Eds.), The Barents Sea Ecosystem, Resources and Management. Tapir Academic Press, Trondheim, pp. 37–76.
Pedersen, T., Mikkelsen, N., Lindstrøm, U., Renaud, P.E., Nascimento, M.C., Blanchet, M.-.A., Ellingsen, I.H., Jørgensen, L.L., Blanchet, H., 2021. Overexploitation, recovery, and warming of the Barents Sea ecosystem during 1950–2013. Front. Mar. Sci. 8 https://doi.org/10.3389/fmars.2021.732637.
Perry, A.L., Low, P.J., Ellis, J.R., Reynolds, J.D., 2005. Climate change and distribution shifts in marine fishes. Science 308, 1912–1915. https://doi.org/10.1126/science.1111322.
Poloczanska, E.S., Burrows, M.T., Brown, C.J., García Molinos, J., Halpern, B.S., Hoegh-Guldberg, O., Kappel, C.V., Moore, P.J., Richardson, A.J., Schoeman, D.S., Sydeman, W.J., 2016. Responses of marine organisms to climate change across oceans. Front. Mar. Sci. 3 https://doi.org/10.3389/fmars.2016.00062.
Polovina, J., 1984. Model of a coral reef ecosystem. Coral Reefs 3, 1–11. https://doi.org/10.1007/BF00306135.
Pörtner, H.-O., Gutt, J., 2016. Impacts of climate variability and change on (marine) animals: physiological underpinnings and evolutionary consequences. Integr. Comp. Biol. 56, 31–44. https://doi.org/10.1093/icb/icw019.
Prokhorova, T. (ed.) 2013. Survey report from the joint Norwegian/Russian ecosystem survey in the Barents Sea and adjacent waters, August-October 2013. 131 pp. 10.13140/RG.2.2.34802.76484.
Prozorkevich, D., van der Meeren, G., Trofimov, A. (eds.) 2020. Survey report from the joint Norwegian/Russian ecosystem survey in the Barents Sea and adjacent waters, 1-2020 ed 93 pp.
Püts, M., Taylor, M., Núñez-Riboni, I., Steenbeek, J., Stäbler, M., Möllmann, C., Kempf, A., 2020. Insights on integrating habitat preferences in process-oriented ecological models—a case study of the southern North Sea. Ecol. Model. 431, 109189 https://doi.org/10.1016/j.ecolmodel.2020.109189.
Reigstad, M., Carroll, J., Slagstad, D., Ellingsen, I., Wassmann, P., 2011. Intra-regional comparison of productivity, carbon flux and ecosystem composition within the northern Barents Sea. Prog. Oceanogr. 90, 33–46. https://doi.org/10.1016/j.pocean.2011.02.005.
Renaud, P.E., Daase, M., Banas, N.S., Gabrielsen, T.M., Søreide, J.E., Varpe, Ø., Cottier, F., Falk-Petersen, S., Halsband, C., Vogedes, D., 2018. Pelagic food-webs in a changing Arctic: a trait-based perspective suggests a mode of resilience. ICES J. Mar. Sci. https://doi.org/10.1093/icesjms/fsy063.
Romagnoni, G., Mackinson, S., Hong, J., Eikeset, A.M., 2015. The Ecospace model applied to the North Sea: evaluating spatial predictions with fish biomass and fishing effort data. Ecol. Model. 300, 50–60. https://doi.org/10.1016/j.ecolmodel.2014.12.016.
RStudio, 2021. RStudio: integrated Development Environment for R in: Team, R. (Ed.), 1.4.1717 ed. RStudio, PBC, Boston, MA.
Schlichtholz, P., 2019. Subsurface ocean flywheel of coupled climate variability in the Barents Sea hotspot of global warming. Sci. Rep. 9, 13692. https://doi.org/10.1038/s41598-019-49965-6.
Skaret, G., Dalpadado, P., Hjøllo, S., Skogen, M., Strand, E., 2014. Calanus finmarchicus abundance, production and population dynamics in the Barents Sea in a future climate. Prog. Oceanogr. 125, 26–39. https://doi.org/10.1016/j.pocean.2014.04.008.
Skjoldal, H., Mundy, P., 2013. Large Marine Ecosystems (LMEs) of the Arctic area. Revision of the Arctic LME map. Retrieved from Akureyri, Iceland. http://hdl.handle.net/11374/61.
Slagstad, D., McClimans, T., 2005. Modeling the ecosystem dynamics of the Barents Sea including the marginal ice zone: I. Physical and chemical oceanography. J. Mar. Syst. 58, 1–18. https://doi.org/10.1016/j.jmarsys.2005.05.005.
Trofimov, A., Karsakov, A., Ivshin, V., 2019. Climate changes in the Barents Sea over the last half century, in: E. Shamray, Huse, G., Trofimov, A., Sundby, S., Dolgov, A., Skjoldal, H.R. et al., Zabavnikov, V. (Eds.), Influence of Ecosystem Changes on Harvestable Resources at High Latitudes 18th Russian-Norwegian Symposium. IMR/PINRO Joint Report Series, Murmansk, Russia, p. 217.
Walters, C., Christensen, V., Pauly, D., 1997. Structuring dynamic models of exploited ecosystems from trophic mass-balance assessments. Rev. Fish Biol. Fish. 7, 139–172. https://doi.org/10.1023/A:1018479526149.
Walters, C., Pauly, D., Christensen, V., 1999. Ecospace: prediction of mesoscale spatial patterns in trophic relationships of exploited ecosystems, with emphasis on the impacts of marine protected areas. Ecosystems 2, 539–554. https://doi.org/10.1007/s100219900101.
Wienerroither, R., Johannesen, E., Dolgov, A., Byrkjedal, I., Bjelland, O., Drevetnyak, K., Eriksen, K., Høines, Å., Langhelle, G., Langøy, H., 2011. Atlas of the Barents Sea Fishes. IMR-PINRO Joint Report Series, pp. 1–272, 1-2011.
Woillez, M., Poulard, J.-.C., Rivoirard, J., Petitgas, P., Bez, N., 2007. Indices for capturing spatial patterns and their evolution in time, with application to European hake (Merluccius merluccius) in the Bay of Biscay. ICES J. Mar. Sci. 64, 537–550. https://doi.org/10.1093/icesjms/fsm025.
Woillez, M., Rivoirard, J., Petitgas, P., 2009. Notes on survey-based spatial indicators for monitoring fish populations. Aquat. Living Resour. 22, 155–164. https://doi.org/10.1051/alr/2009017.
Wolodzko, T., 2019. R package version 1.8.11.
Zar, J.H., 1998. Biostatistical Analysis, 4th ed. Prentice Hall, Upper Saddle River, N.J.